



Defence Research and
Development Canada

Recherche et développement
pour la défense Canada



Prediction of Image Registration Performance

Final Report

Vincent Labbé
AEREX Avionics Inc.

The scientific or technical validity of this contract report is entirely the responsibility of the contractor and the contents do not necessarily have the approval or endorsement of the Department of National Defence of Canada.

Defence Research and Development Canada – Valcartier

Contract Report
DRDC Valcartier CR 2013-036
March 2012

Canada

Prediction of Image Registration Performance

Final Report

Vincent Labbé
AEREX Avionics Inc.

Prepared by:
AEREX Avionics Inc.
324, Saint-Augustin Avenue
Breakeyville (Québec) G0S 1E1

Contractor's document number: 2011-92854-2
Contract project manager: Paul Lacasse, 418-832-1040
PWGSC contract number: W7701-092854/001/QCL
CSA: François Leduc, Defence scientist, 418-844-4000 x4703

The scientific or technical validity of this contract report is entirely the responsibility of the contractor and the contents do not necessarily have the approval or endorsement of the Department of National Defence of Canada.

Defence Research and Development Canada – Valcartier

Contract Report
DRDC Valcartier CR 2013-036
March 2012

IMPORTANT INFORMATIVE STATEMENTS

The scientific or technical validity of this contract report is entirely the responsibility of the contractor and the contents do not necessarily have the approval or endorsement of the Department of National Defence of Canada.

© Her Majesty the Queen in Right of Canada, as represented by the Minister of National Defence, 2012.

© Sa Majesté la Reine (en droit du Canada), telle que représentée par le ministre de la Défense nationale, 2012.

Abstract

This report presents a practical method for estimating registration mapping error for a given relief and satellite attitudes. This method relies on a simulation using a digital elevation model to calculate the mapping error for a set of parameters. The method was applied to a test set of digital elevation models showing diverse terrain reliefs: flat, pretty flat, mountainous, and mountainous near a coast. Mapping error increases for terrains with more relief; but this error can be reduced by using local mapping algorithms, which were found to decrease mapping error for mountainous regions by 80%. Our method quantifies the mapping error and compares the mapping error for diverse conditions. These results can then be used to delimit the change detection capability and to better plan future image acquisition missions.

Résumé

Ce rapport présente une méthode permettant d'estimer l'erreur de mappage, lors du recalage, pour un relief et des positions de satellite donnés. Cette méthode se base sur une simulation utilisant un modèle altimétrique numérique afin de calculer l'erreur de mappage pour un ensemble de paramètres. Cette méthode fût appliquée à un ensemble de modèles altimétriques numériques de test comportant divers types de reliefs : plat, presque plat, montagneux, montagneux près d'une côte. Évidemment, l'erreur de mappage croît pour les terrains comportant plus de relief, mais cette erreur peut être réduite en utilisant des algorithmes de mappage local. On a estimé que les algorithmes de mappage local font diminuer l'erreur de mappage dans les régions montagneuses de 80%. Notre méthode permet de quantifier l'erreur de mappage et de comparer les erreurs de mappage pour différentes conditions. Ces résultats peuvent alors servir à délimiter les capacités des algorithmes de détection de changement et à mieux planifier de futures missions d'acquisition de données.

This page intentionally left blank.

Executive summary

Prediction of Image Registration Performance: Final Report

Vincent Labbé; DRDC Valcartier CR 2013-036; Defence Research and Development Canada – Valcartier; March 2012.

Introduction or background: Accurate change detection is of prime interest for military surveillance. Remote sensing is a key source of data for change detection; but these data are challenging in many ways: difference in illumination and angles of view, deformation due to image acquisition, cloud cover. Relief causes image deformation during the image formation process, and is a known source of registration error. Actually, this deformation makes the mapping function between two images particularly difficult to estimate, and prone to errors. These errors eventually result in false alarms in a change detection process. This report presents a practical method for estimating registration mapping error for a given relief, satellite positions and viewing directions. This method relies on a simulation using a digital elevation model to calculate the mapping error for a set of parameters.

Results: This method was applied to a test set of digital elevation models showing diverse terrain reliefs: flat, pretty flat, mountainous, and mountainous near a coast. Mapping errors were evaluated for four classical mapping algorithms: projective, polynomial, polynomial with image partitioning, and piecewise linear. This experiment aimed at finding the best algorithm for each situation. For less than 400 ground control points (GCPs), a polynomial of second order mapping algorithm is in most cases the best choice, with projective mapping not very far. For more than 400 GCPs, local mapping algorithms are best suited, especially piecewise linear mapping. As relief increases, so does the mapping error; but this is alleviated as the number of GCPs gets higher. Local mapping methods (polynomial with image partitioning and piecewise linear) have been shown to reduce the mapping error by more than 80% for mountainous reliefs. Moreover, for a very large number of GCPs, mapping error for terrains with relief can be reduced to levels similar to flat terrains.

Significance: Our method allows us to quantify the mapping error and to compare the mapping error for diverse conditions. These results can then be used to delimit the change detection capability and to better plan future image acquisition missions. By selecting pair of images with low mapping error, the number of false alarms will be reduced. This approach could enable automatic processing of a lot of presently unused data.

Future plans: The second part of this project will integrate the mapping estimation algorithm into a suite of tools to plan future acquisitions and to select pair of images adequate for change detection. The selected pair of images will be fed to change detection algorithms. This work will result in a practical change detection tool that will use filtered data as input

Sommaire

Prediction of Image Registration Performance: Final Report

Vincent Labbé ; DRDC Valcartier CR 2013-036 ; Recherche et développement pour la défense Canada – Valcartier ; mars 2012.

Introduction ou contexte : La détection de changement est d'un grand intérêt pour les opérations de surveillance militaire. La télédétection est une source privilégiée de données pour la détection de changement, mais le traitement de ces données présente plusieurs défis : différence d'illumination et d'angles de vue, déformation lors de l'acquisition, couvert nuageux. Le relief de la zone observée est une cause de déformation lors de la génération de l'image, donc une source d'erreur pour l'étape de recalage. En fait, cette déformation rend la fonction de mappage difficile à évaluer, ce qui cause des erreurs de recalage, et des fausses alarmes lors de l'application de processus de détection de changement. Ce rapport présente une méthode permettant d'estimer l'erreur de mappage, lors du recalage, pour un relief, des positions et des prises de vue de satellite données. Cette méthode se base sur une simulation utilisant un modèle altimétrique numérique afin de calculer l'erreur de mappage pour un ensemble de paramètres.

Résultats : Cette méthode fût appliquée à un ensemble de modèles altimétriques numériques comportant divers types de reliefs : plat, presque plat, montagneux, montagneux près d'une côte. L'erreur de mappage fut évaluée pour quatre algorithmes de mappage classiques : projective, polynomial, polynomial avec partition de l'image, linéaire par morceaux. Ce test vise à déterminer le meilleur algorithme pour chaque situation. Lorsque moins de 400 points d'appui au sol (GCP) sont disponibles, l'algorithme polynomial de second ordre donne le plus souvent le meilleur résultat, l'algorithme projectif n'étant pas très loin. Lorsque plus de 400 GCPs sont disponibles, les algorithmes de mappage locaux sont les mieux adaptés, en particulier celui linéaire par morceaux. L'erreur de mappage croît lorsque le relief est plus grand, mais cette erreur peut grandement être réduite en augmentant le nombre de GPCs. Les algorithmes de mappage locaux (polynomial avec partition de l'image et linéaire par morceaux) ont démontrés une réduction de l'erreur de mappage de plus de 80% pour des reliefs montagneux. En plus, pour un très grand nombre de GCPs, l'erreur de mappage pour les terrains avec relief peut être ramenée à un niveau similaire à celle pour les terrains plats.

Importance : Notre méthode permet de quantifier l'erreur de mappage et de comparer les erreurs de mappage pour différentes conditions. Ces résultats peuvent alors servir à délimiter les capacités des algorithmes de détection de changement et à mieux planifier de futures missions d'acquisition. En sélectionnant les paires d'images avec une faible erreur de mappage, le nombre de fausses alarmes peut être réduit. Cette réduction pourrait permettre un traitement automatique exploitant ainsi un grand nombre d'images présentement inutilisées.

Perspectives : Dans la seconde partie de ce projet, on procédera à l'intégration de l'algorithme d'estimation de l'erreur de mappage dans une collection d'outils permettant de planifier des missions d'acquisition et de sélectionner les paires d'images adéquates pour la détection de changement. Ces paires d'images serviront d'entrées pour des algorithmes de détection de changement. Ceci résultera en un outil de détection de changement prenant en entrée des données sélectionnées pour une performance optimale.

Table of contents

Abstract	i
Résumé	i
Executive summary	iii
Sommaire	iv
Table of contents	v
List of figures	vii
List of tables	viii
Acknowledgements	ix
1 Introduction.....	1
2 Image registration	2
3 Dataset	3
4 Occlusion detection.....	6
4.1 Introduction	6
4.2 Definitions	6
4.3 Ray casting	8
4.4 Implementation.....	11
4.5 Results	11
5 Mapping error evaluation.....	12
5.1 Introduction	12
5.2 Methodology	12
5.2.1 Define 2D Ground Control Points and Test Points	13
5.2.1.1 2D GCPs selection.....	13
5.2.1.2 2D TPs selection.....	14
5.2.2 3D control points coordinates	15
5.2.2.1 3D GCPs coordinates.....	15
5.2.2.2 3D TPs coordinates.....	16
5.2.3 Remove occluded points	16
5.2.4 Projected to camera plane	17
5.2.5 Estimate mapping function	17
5.2.5.1 Global mapping	18
5.2.5.2 Local mapping.....	19
5.2.6 Calculate mapping error on TPs.....	20
5.3 Function for getting mapping error	21
5.4 Results	22
6 Conclusion	28
References	29

Annex A .. Effet of Earth curvature on simulation	31
A.1 Satellite position	31
A.2 Digital elevation model	32
Annex B... Results	35
B.1 Number of partitions.....	35
B.2 Number of points.....	35
B.2.1 Small number of GCPs.....	36
B.2.2 Large number of GCPs.....	37
List of symbols/abbreviations/acronyms/initialisms	41

List of figures

Figure 1: Occlusion definition.....	6
Figure 2: Ray casting example	8
Figure 3: Ray casting example - projection and intersection points.....	9
Figure 4: Ray casting example - compare line of sight height to ground elevation	9
Figure 5: Ray casting example - result	10
Figure 6: Example occlusion image obtained with ray casting	10
Figure 7: Mapping error evaluation geometry.....	12
Figure 8: Mapping error evaluation methodology.....	13
Figure 9: 2D GCPs - grid selection example ($20 \times 20 = 400$ points)	14
Figure 10: 2D GCPs - random selection example ($20 \times 20 = 400$ points)	14
Figure 11: 2D TP selection example (1000 points)	15
Figure 12: 3D GCPs - grid selection example ($20 \times 20 = 400$ points)	15
Figure 13: 3D GCPs - random selection example ($20 \times 20 = 400$ points)	16
Figure 14: 3D TP selection example (1000 points)	16
Figure 15: Pinhole camera model.....	17
Figure 16: Polynomial mapping with image partitioning.....	20
Figure 17: Piecewise linear mapping.....	20
Figure 18: Mapping error vs. number of partitions	23
Figure 19: Mapping error vs. number of GCPs (few points).....	24
Figure 20: Mapping error vs. number of control points (many points)	25
Figure 21: Best mapping error vs. number of GCPs (grid selection)	26
Figure 22: Best mapping error vs. number of GCPs (random selection)	27
Figure A-1: Satellite position considering Earth curvature	31
Figure A-2: Satellite distance using law of cosines.....	32
Figure A-3: Earth curvature effect on ground elevation values	33

List of tables

Table 1: Digital elevation models description	3
Table 2: Digital elevation models location and image	4
Table 3: Number of occluded points vs. satellite zenith angle	11
Table 4: Mapping error – relief vs. no relief	27
Table B-1: Estimated mapping error vs. Number of partitions	35
Table B-2: Estimated mapping error for DEM 1 – small number of GCPs	36
Table B-3: Estimated mapping error for DEM 2 – small number of GCPs	36
Table B-4: Estimated mapping error for DEM 3 – small number of GCPs	36
Table B-5: Estimated mapping error for DEM 4 – small number of GCPs	37
Table B-6: Estimated mapping error for DEM 1 – large number of GCPs	37
Table B-7: Estimated mapping error for DEM 2 – large number of GCPs	38
Table B-8: Estimated mapping error for DEM 3 – large number of GCPs	38
Table B-9: Estimated mapping error for DEM 4 – large number of GCPs	39

Acknowledgements

The author would like to thank Dr. Pierre Lahaie for his scientific direction in developing the experimentation, and for reviewing the results and the report.

The author would like to thank Dr. François Leduc for continuous supervision and insights.

The author also thanks Vincent Rivet and Nicolas Bédard-Maltaïs for their advice on implementing the algorithms.

This page intentionally left blank.

1 Introduction

Accurate change detection is of prime interest for military surveillance operation. Remote sensing is a key source of data for change detection, but these data are challenging in many ways. Differences in illumination and angles of view, deformations due to image acquisition and cloud cover can hinder using remotely sensed data for surveillance. This project aims at optimising the use of remote sensing data in the context of change detection. First, input image data will be filtered, or their acquisition planned, according to the capability of change detection algorithms. For example, a pair of images taken at very different view angles could be rejected. Second, change detection algorithms will be implemented to process this filtered data.

Image registration is usually the first step in a chain of algorithms towards change detection. Image registration transforms data from one image into the coordinate system of another image. This allows comparing images point to point. Registration errors can be reported as change in a change detection context, consequently generating false alarms. It is therefore necessary to limit this error as much as possible.

Relief causes image deformation during the image formation process, and is a known source of registration error. Actually, this deformation makes the mapping function between two images particularly difficult to estimate, and prone to errors. Some work has been done on the assessment of registration error in mountainous area [1] and on dealing with this problem [2, 3], but a thorough characterisation of the impact of relief on registration mapping error was not found in the scientific literature.

This report presents a practical method for estimating mapping error for a given relief, satellite positions and viewing directions. This method relies on a simulation using a digital elevation model to calculate the mapping error for a set of parameters. These results can then be used to delimit the change detection capability and to better plan future image acquisition missions.

This project is divided into two parts. The first part, presented in this report, characterises registration mapping error for a pair of images. This information is useful to select a registration algorithm, to decide if a pair of images is suitable for change detection, and to improve future image acquisition missions planning. The second part will implement a working change detection algorithm by using the results of the first part to filter input data. Change detection algorithms can therefore be designed for manageable cases, and are expected to yield better detection results.

This report presents a method for estimating mapping error for a pair of images. Section 2 briefly introduces image registration and the errors involved in this operation. Section 3 describes the digital elevation models used as a test dataset for our method. Section 4 presents occlusion detection as a necessary step of our method. Section 5 details each step of the mapping error evaluation process, and the results of applying this process to our test set. Section 6 draws overall conclusions over the method and results.

2 Image registration

Image registration is the alignment of two or more images into the same coordinate system. In practice, if two images are to be compared, data from one image (sensed image) is transformed into the coordinate system of the other image (reference image).

Image registration methods have been extensively reviewed by Brown [4], Zitova and Flusser [5], and more recently by Wyawahare et al.[6]. Existing image registration techniques fit into a generic frame, where an image transformation model is estimated from sets of so-called control points.

The generic image registration process can be divided into three steps:

1. Ground control points (GCPs) selection and matching
2. Mapping estimation
3. Image transformation

GCPs selection and matching consist in selecting, in the sensed image and the reference image, 2D points referring to the same 3D reality. Mapping estimation uses these GCPs to estimate a transformation from 2D points in sensed image to 2D points in reference image. Image transformation applies the mapping to transform the content of the sensed image into the coordinate system of the reference image.

There are numerous sources of error along the image registration process:

1. Precision of GCPs: corresponding GCPs may not precisely indicate the same 3D position. Note that this imprecision can originate from many causes.
2. Matching of GCPs: GCPs from sensed image can be incorrectly paired to GCPs from reference image.
3. Mapping error: the chosen transformation model and parameters may not perfectly transform GCPs from sensed image into GCPs from reference image. Usually, this error is minimised using a least-square approximation.
4. Interpolation error in image content transformation: transformation of the sensed image into the coordinates of the reference image may introduce errors as interpolation is often needed.

Presence of relief in the observed area puts emphasis on the mapping error, since it becomes challenging to find an adequate transformation model, and many GCPs are needed to infer a complex mapping function.

3 Dataset

Digital elevation models for our test dataset were taken from Geobase [7], a Canada governments' initiative supervised by the Canadian Council on Geomatics (CCOG). The Geobase website provides access to Canadian Digital Elevation Data (CDED) [8], which consists of uniformly-spaced arrays of ground elevations, available at scales 1:50 000 (used here) and 1: 250 000. CDED files are separated into Western and Eastern sections. Ground elevations are given in metres relative to Mean Sea Level, based on the North American Datum 1983 (NAD83).

Our test dataset consisted of four digital elevation models showing dissimilar types of relief. Each digital elevation model is an array of 1201 by 1201 integer values. The grid resolution is around 20 metres. Table 1 gives the location of each digital elevation model in the test set and presents relief-descriptive statistics (in metres). Table 2 shows the digital elevation models along their geographical locations on a map. Images in both tables have x and y scales in pixels (1 pixel \approx 20 metres), and z scale in metres. Note that these scales exaggerate the aspect of relief.

Table 1: Digital elevation models description

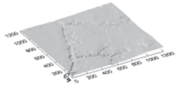
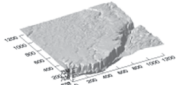
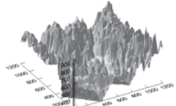
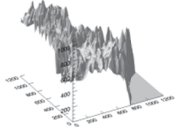
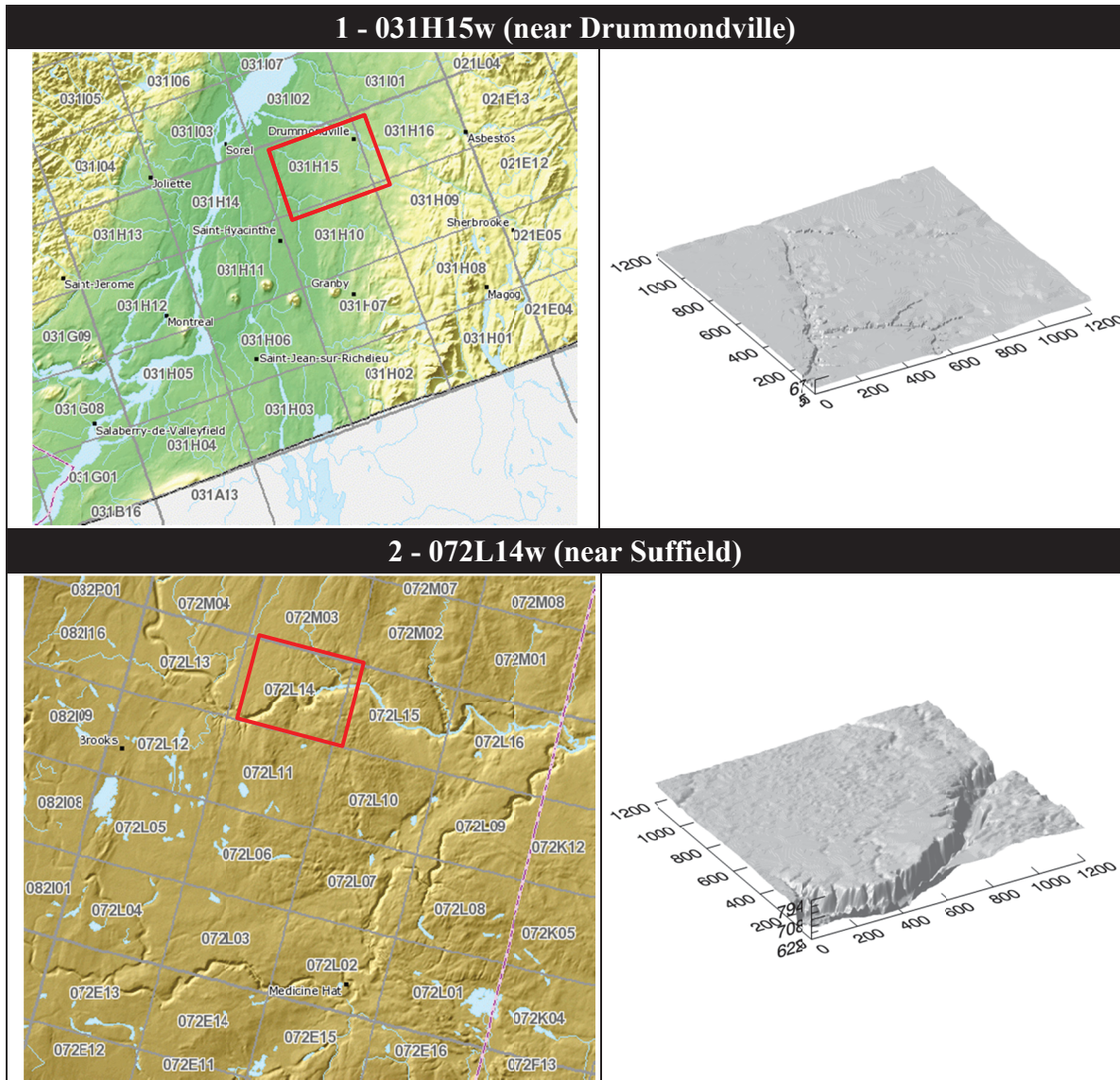
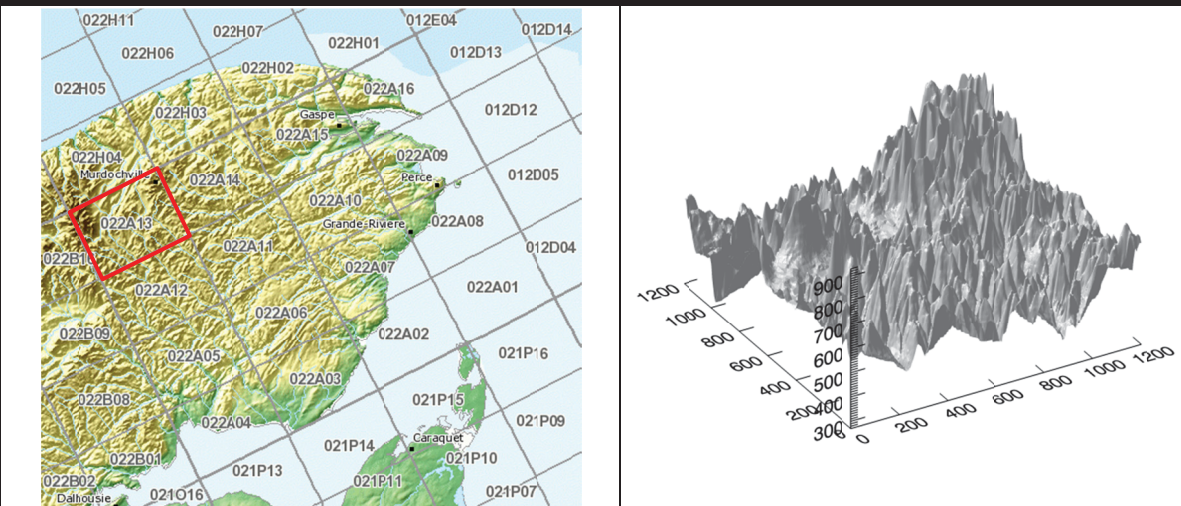
No	Location	Name	Min	Max	Mean	Std Dev	Image
1	Centre-du-Québec, near Drummondville, Quebec, Canada	031H15w	5	67	32.3	9.484	
2	Alberta South, Near Suffield Base, Alberta, Canada	072L14w	622	794	718.1	29.75	
3	Gaspésie, near Murdochville, Quebec, Canada	022A13e	270	931	588.0	100.2	
4	Charlevoix, near Baie St-Paul, Quebec, Canada	021M07e	4	1091	475.8	277.6	

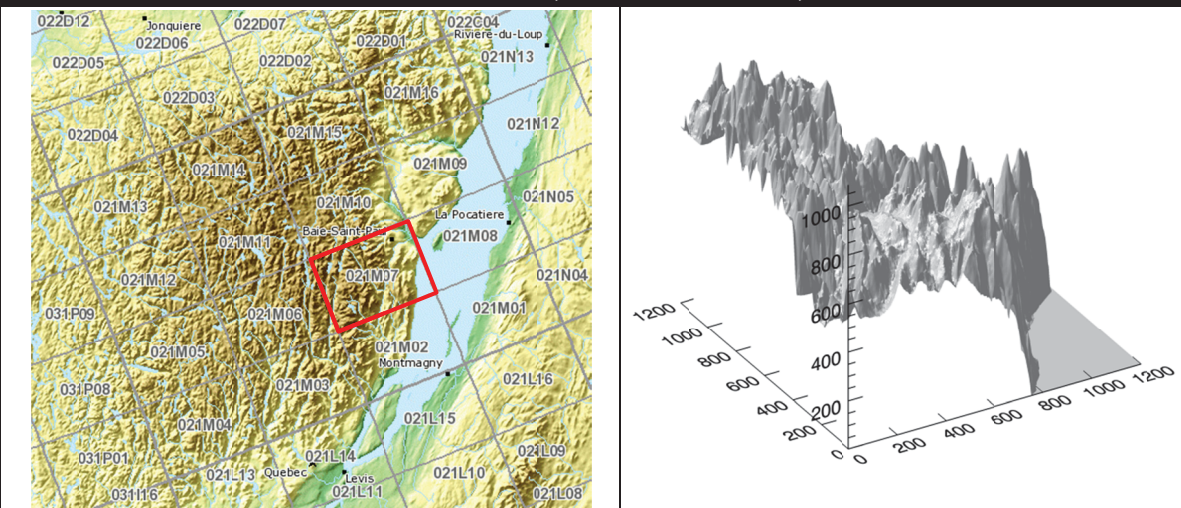
Table 2: Digital elevation models location and image



3 - 022A13e (near Murdochville)



4 - 021M07e (near Baie St-Paul)



4 Occlusion detection

4.1 Introduction

Due to terrain relief and sensor viewing angle, some ground surface may not be visible in a remotely sensed image. This hidden surface clearly sets an upper bound on change detection since no conclusion can be drawn about that surface. Moreover, it can impair image registration since visible ground surface can vary for different viewpoints. It is therefore necessary to evaluate hidden ground surface to take it into account, and to set bounds on registration error and change detection performance.

The approach taken to evaluate visible and hidden ground surface is to simulate the sensor view using a digital elevation model. This approach is discussed in the following subsections. Section 4.2 gives definitions concerning occlusion. Section 4.3 presents ray casting as an algorithm for occlusion detection. Section 4.4 discusses the implementation of the ray casting algorithm. Section 4.5 presents results obtained by applying occlusion detection on the previously described test dataset (section 3). Finally, conclusions are drawn concerning the use of occlusion detection in the context of change detection.

4.2 Definitions

Visibility can be defined operationally as: A line of sight from sensor to surface point, which is not obstructed. In figure 1, points A, B, C, D, E and F are ground points; point S is the imaging sensor position (also called viewpoint in this report). Points A, B, D, E and F are visible; point C is occluded because it is not visible from S : its line of sight is obstructed.

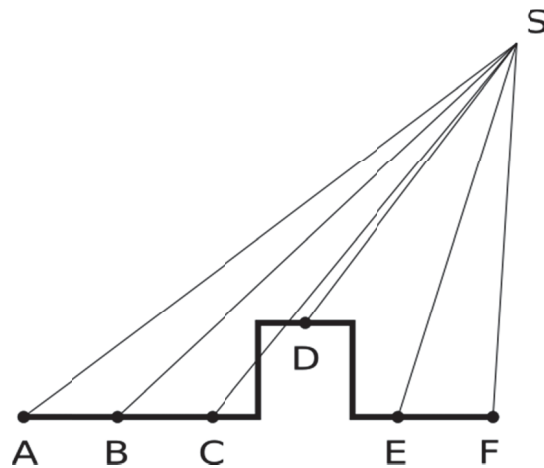


Figure 1: Occlusion definition

Let Z be a $L_x \times L_y$ grid of uniformly-spaced ground elevation values $z_{i,j}$, $1 \leq i \leq L_x$, $1 \leq j \leq L_y$ (L_x being the grid width and L_y the grid height). We denote the set of visible ground points from viewpoint n as

$$V_n = \{ z_{i,j} \in Z \mid z_{i,j} \text{ is visible from viewpoint } n \} \quad (1)$$

where viewpoint is a position above the grid, defined as a 3-dimension coordinate.

We define coverage as the ratio of the number of visible points to the total number of points; formally, for viewpoint a ,

$$\text{coverage}(a) = \frac{|V_a|}{|Z|} \quad (2)$$

Occlusion is defined as the complement of coverage, i.e. the ratio of the number of hidden points to the total number of points; formally,

$$\text{occlusion}(a) = \frac{|Z| - |V_a|}{|Z|} \quad (3)$$

In the context of change detection, two images are acquired at different times and from possibly different viewpoints. Hence, there are two possible different sets of visible points. By definition, a point has to be visible from both viewpoints to serve for change detection. Pair coverage, formally defined below, measures the ratio of points visible from both viewpoints. Pair coverage can be seen as a fitness criterion of an image pair for change detection in the view of occlusion.

$$\text{pair coverage}(a, b) = \frac{|V_a \cap V_b|}{|Z|} \quad (4)$$

The preceding concepts describe the surface that is covered from a viewpoint, or from a pair of viewpoints. When it comes to mapping points from one image to another, as in image registration, we are interested in knowing, which points appear on the first image but not on the other. Let differential coverage be the ratio of points visible from viewpoint a that can be mapped onto points visible from viewpoint b , on the number of points visible from a :

$$\text{differential coverage}(a \rightarrow b) = \frac{|V_a \cap V_b|}{|V_a|} \quad (5)$$

Differential occlusion is the ratio of the number of points visible from viewpoint a but not visible from viewpoint b , on the number of points visible from a :

$$\text{differential occlusion}(a \rightarrow b) = \frac{|V_a \setminus V_b|}{|V_a|} \quad (6)$$

4.3 Ray casting

There exist many techniques for hidden surface detection. Z-buffering [9-11], which deals with geometric objects defined in 3D continuous coordinates, has been adapted to the context of discrete 2.5D data provided by digital elevation models [12-14]. Habib et al.[15] have shown the limits of the Z-buffer technique in this context and have proposed an angle of view-based method. We have chosen to use the ray casting algorithm [16], which yields the same results.

Since ground elevation is represented as a discrete grid, and coordinates as continuous values, we consider each ground elevation value to be the center of a 1×1 square of equal value, and we only test this center for visibility. Consequently, in our approximation, a ground elevation value from a digital elevation model is considered visible if its center is visible.

Ray casting determines the visibility of point A from viewpoint S by finding the first intersection of a ray cast from S to A ; if A is the first intersection, it is visible, otherwise it is occluded. This algorithm is illustrated using a simple example, shown in figure 2. Point A is tested for occlusion from viewpoint S .

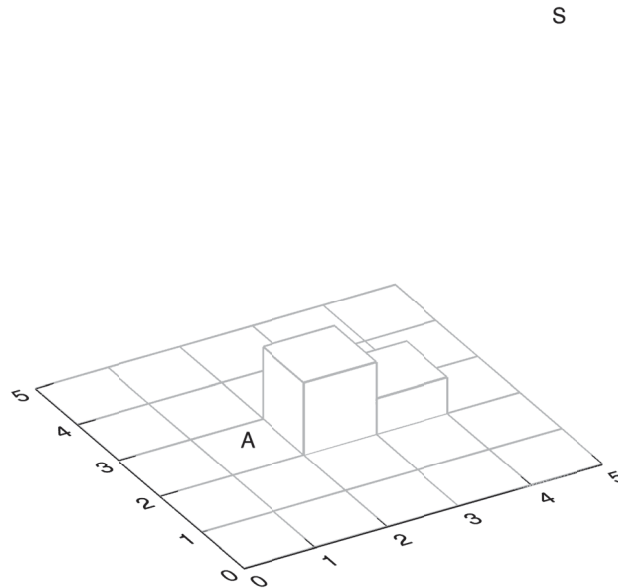


Figure 2: Ray casting example

First, the line of sight between viewpoint S and point A is projected onto the digital elevation model plane to give intersection points marked by an X (see figure 3).

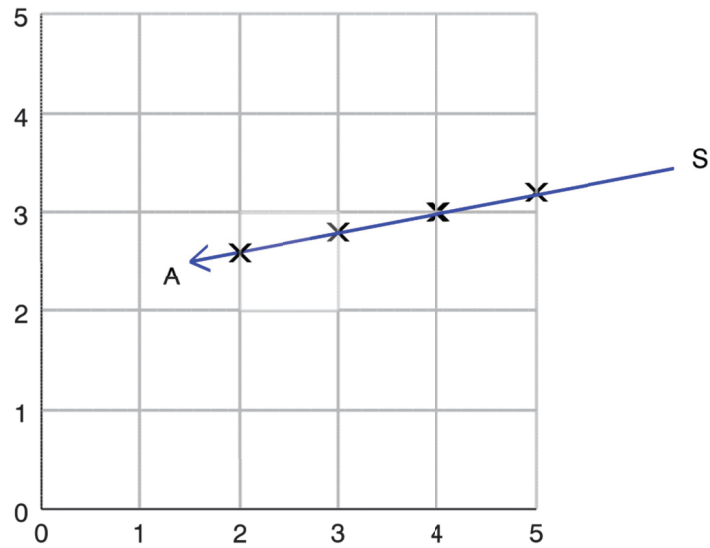


Figure 3: Ray casting example - projection and intersection points

At each of these points, line of sight height is compared to ground elevation. Figure 4 shows line of sight height (blue line) versus ground elevation at test points (black rectangles). Point *A* is occluded since ground elevation of its first neighbour is greater than the height of the line of sight (figure 5). These steps are repeated for every point of the digital elevation model, resulting in an occlusion mask.

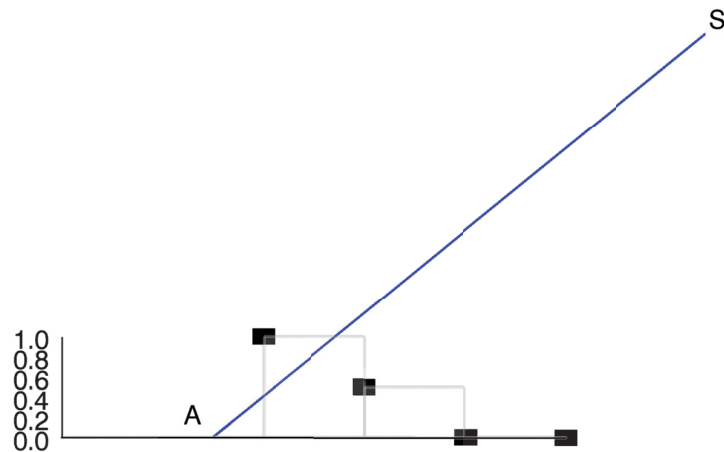


Figure 4: Ray casting example - compare line of sight height to ground elevation

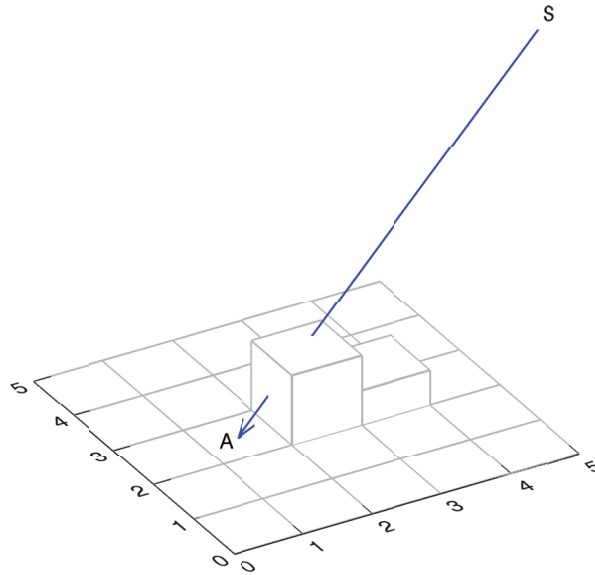


Figure 5: Ray casting example - result

Figure 6 shows a visualisation of occlusion detection performed with ray casting. The dotted red line displays the line of sight from satellite position to digital elevation model center at zero ground elevation. Ground elevations are showed as a surface overlaid with the calculated occlusion mask, also showed as a 2D image at ground elevation 550 m.

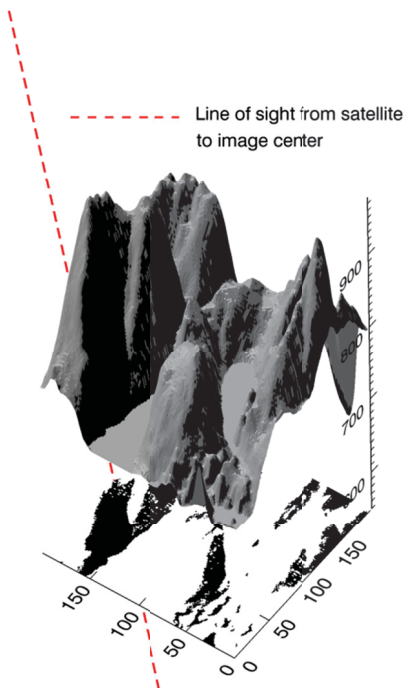


Figure 6: Example occlusion image obtained with ray casting

4.4 Implementation

Ray casting was implemented in IDL [17]. It was optimised to use IDL parallel operations. It takes around 900 seconds on a dual-Xeon 3.4 GHz to calculate occlusion using ray casting IDL implementation for a specific digital elevation model, azimuth and zenith. IDL multithreading capability, named IDL Threadpool, was found to slightly degrade performance when used with 3 threads (1000 seconds). If it were necessary to accelerate ray casting processing in order to give an answer more rapidly or to simulate for a large range of azimuth and zenith values, GPULib [18] from TxCorp could provide an affordable and easy-to-implement solution. GPULib provides CUDA-enabled [19] versions of common IDL array operations, thus enabling to use the Graphics Processing Unit as a coprocessor for compute intensive array operations.

4.5 Results

Occlusion detection was performed on our test set assuming a satellite altitude of 450 000 meters above mean sea level and zenith values of 0, 5, 10, 15, 20, 25, 30, 35, 40, 45 degrees.

Table 3 shows the number of occluded points versus satellite zenith angle for an azimuth of 0 degree, for each digital elevation model of our test set. Without surprise, the number of occluded points gets larger as the zenith angle increases, and is larger for digital elevation model describing regions with more relief.

Using the results in Table 3, we calculate occlusion, which, even for the highest value (DEM 3, 45 degrees) is only 0.00769. Therefore, occlusion can be neglected for our test set. However, these numbers should be considered as minima, since the digital elevation models of our test set have a resolution of about 20 m, which is sufficient for modeling elevation of rather large structures but neglect smaller relief changes. Occlusion would rise sharply for digital elevation models of higher resolutions.

Table 3: Number of occluded points vs. satellite zenith angle

Zenith (deg)	DEM 1	DEM 2	DEM 3	DEM 4
0	0	0	0	0
5	0	0	0	0
10	0	0	0	0
15	0	0	0	0
20	0	0	0	0
25	0	0	41	0
30	0	0	278	11
35	0	0	954	192
40	0	0	3274	911
45	0	5	11094	2915

5 Mapping error evaluation

5.1 Introduction

This section presents a methodology for evaluating the mapping error in the context of remote sensing change detection, i.e. for two images of the same scene taken at different times and view angles. This methodology is then applied to the test set described in section 3.

5.2 Methodology

Mapping error is estimated by simulating image acquisition. Figure 7 presents the geometry of the mapping error simulation. An imaging system, here modeled by a pinhole camera, looks at the ground (digital elevation model) from a viewpoint (defined by altitude, zenith and azimuth).

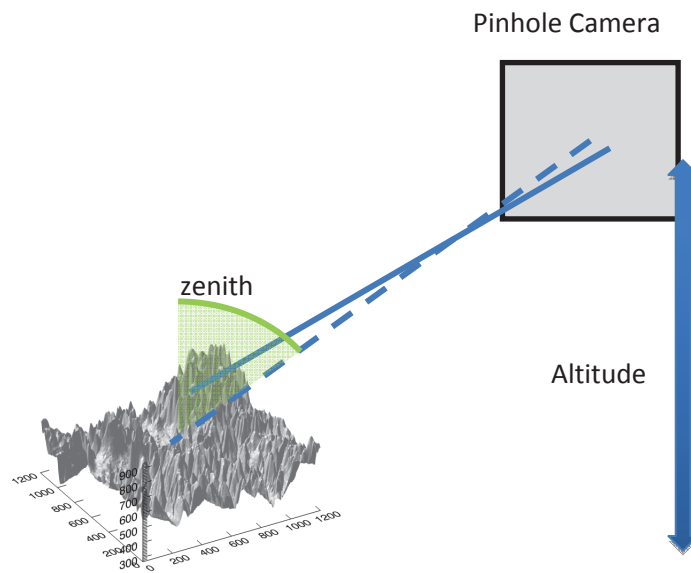


Figure 7: Mapping error evaluation geometry

Mapping error simulation is done in six steps, as summarised in figure 8, and presented in details in the following subsections. First, 2D Ground Control Points (GCPs) and Test Points (TPs) coordinates are defined. Then, the 3D coordinates of those points are found by taking the elevation value of the digital elevation model. For each viewpoint (typically two in change detection), occluded points are removed and the remaining 3D points are projected onto the 2D camera plane using the pinhole camera model. At this stage, there are four sets of 2D points: Ground Control Points (GCPs) and Test Points (TPs) for viewpoint 1, and GCPs and TPs for viewpoint 2. Using the two sets of GCPs, a mapping function is estimated. The mapping error is then evaluated using the two sets of TPs.

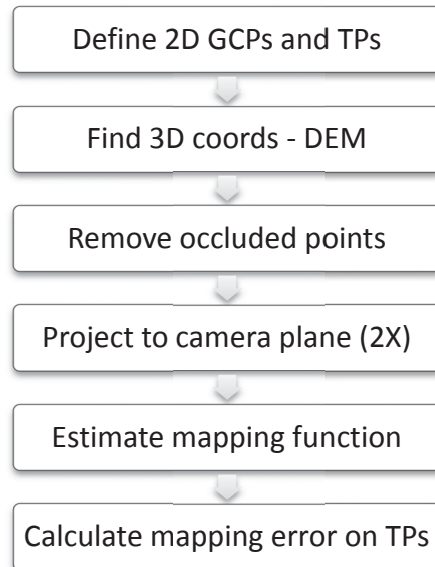


Figure 8: Mapping error evaluation methodology

5.2.1 Define 2D Ground Control Points and Test Points

5.2.1.1 2D GCPs selection

GCPs were selected using two methods: a 2D-grid and randomly. A grid ensures that more points imply a better coverage. Random selection avoids optimistic error evaluation for local mapping methods that depend on coverage.

Figure 9 shows an example 20×20 grid of GCPs for an input image of 1201×1201 values. Figure 10 shows a random selection of 400 points for the same input image.

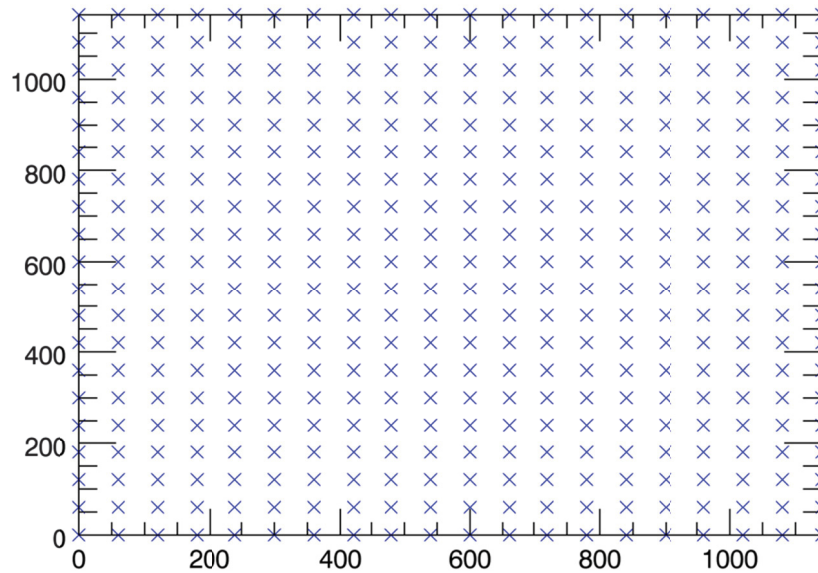


Figure 9: 2D GCPs - grid selection example ($20 \times 20 = 400$ points)

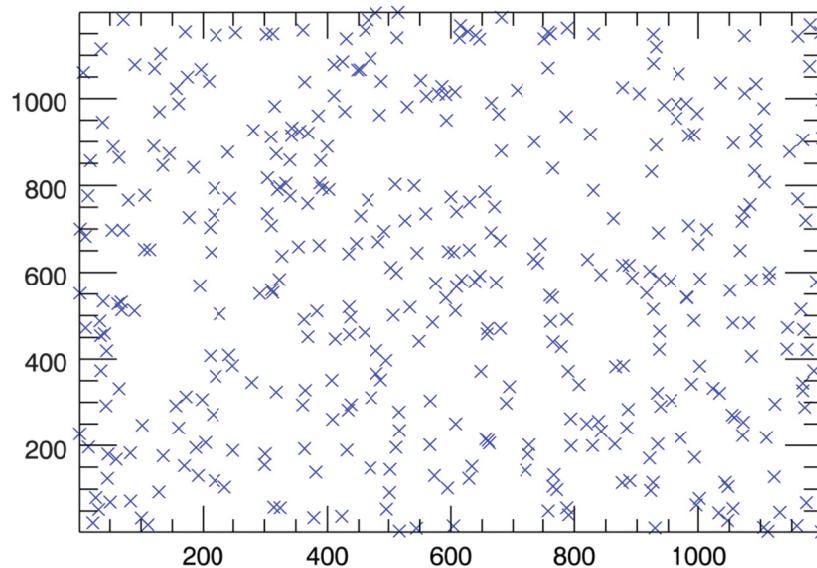


Figure 10: 2D GCPs - random selection example ($20 \times 20 = 400$ points)

5.2.1.2 2D TPs selection

TPs were randomly selected. They are randomly selected to get points near and far the GPCs. A grid of TPs could introduce a bias. Figure 11 shows 1000 2D TPs selected for an input image of 1201×1201 values.

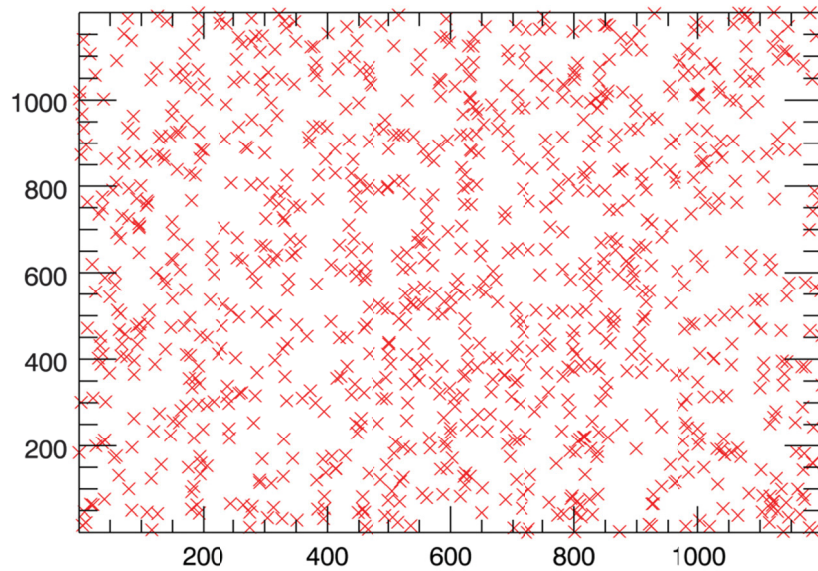


Figure 11: 2D TPs selection example (1000 points)

5.2.2 3D control points coordinates

5.2.2.1 3D GCPs coordinates

3D GCPs are found by taking the digital elevation model (DEM) height values corresponding to previously selected 2D GCPs. Figure 12 shows 3D GCPs found using the example 2D grid points and height values from DEM 3 of our test set (section 3). Figure 13 shows 3D GCPs obtained by random selection.

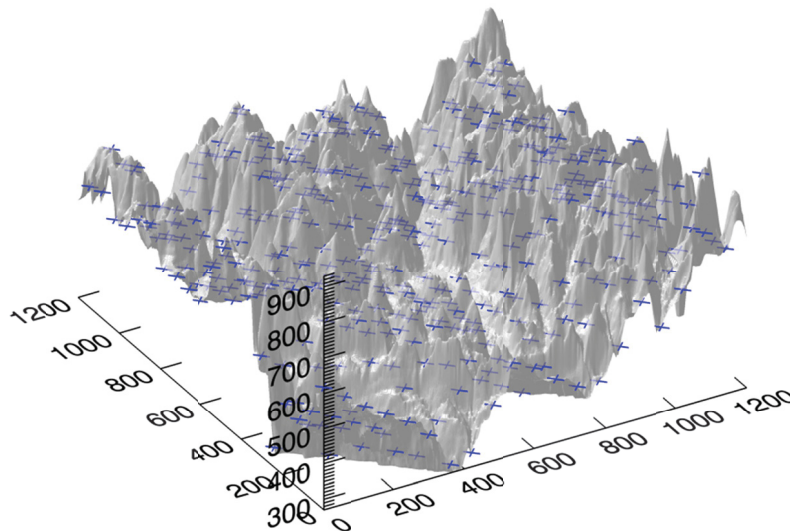


Figure 12: 3D GCPs - grid selection example ($20 \times 20 = 400$ points)

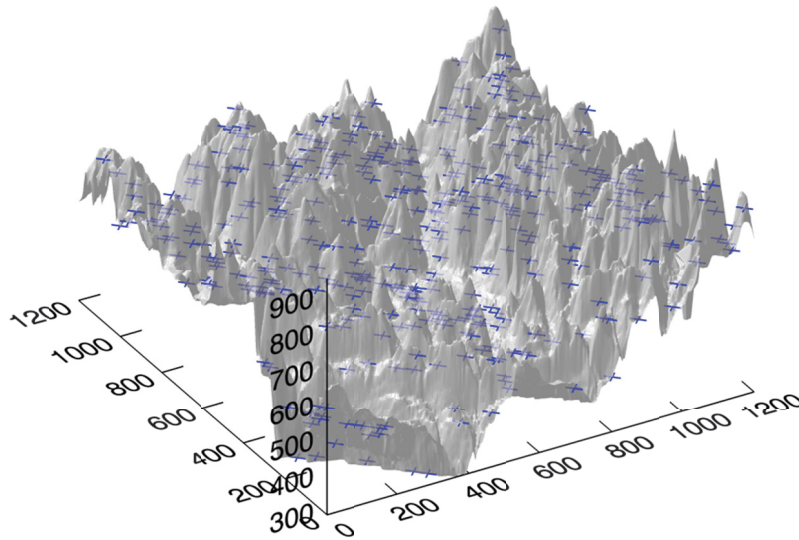


Figure 13: 3D GCPs - random selection example ($20 \times 20 = 400$ points)

5.2.2.2 3D TPs coordinates

3D TPs are found by taking the DEM height values corresponding to 2D TPs. Figure 14 shows 3D TPs found using the example 2D TPs and height values from DEM 3.

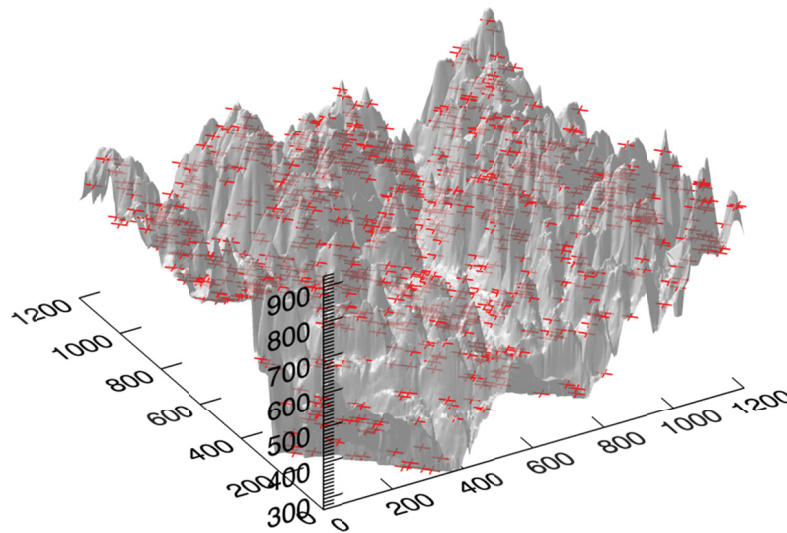


Figure 14: 3D TPs selection example (1000 points)

5.2.3 Remove occluded points

For both viewpoints, occlusion detection is performed using the algorithm described in section 4. Pairs of points containing an occluded point are removed, i.e. are not used for mapping error

AERE

evaluation. This underestimates mapping error since occluded points would actually be replaced by their occluding points, thus misguiding mapping function parameters estimation. However, there is no obvious way to integrate the error generated by occlusion in the mapping error. It was therefore decided to consider it separately.

5.2.4 Projected to camera plane

A pinhole camera model is used to project 3D points to the 2D camera plane. Figure 15, obtained from a report by Obeysekera [20], depicts the geometry of projective transformation using a pinhole camera model. More details on the pinhole camera model can be found in image processing books, such as [21] and [22].

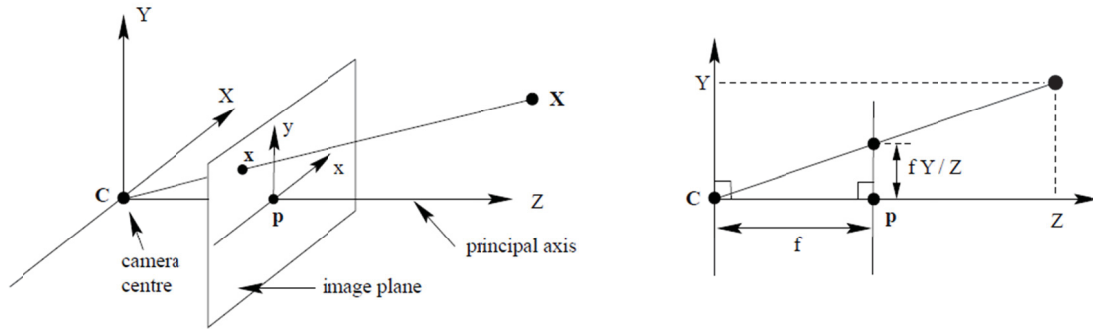


Figure 15: Pinhole camera model

Projected x, y 2D coordinates of X, Y, Z 3D coordinates are found by, (f being the focal length),

$$x = f \frac{X}{Z} \quad (7)$$

$$y = f \frac{Y}{Z} \quad (8)$$

5.2.5 Estimate mapping function

Many methods are available to infer a mapping function between two sets of points [4-6]. We have chosen to implement only the most common methods, which are also used very often. These methods are divided into two groups: global mapping methods and local mapping methods. Global mapping methods use all GCPs at the same time to estimate a mapping function for the whole image. On the other hand, local mapping methods divide the image into regions, and find a mapping for each region by using the GPCs from that region.

In the following mapping methods descriptions, (x, y) represents a coordinate in the sensed image and (X, Y) a coordinate in the reference image.

5.2.5.1 Global mapping

5.2.5.1.1 Projective mapping

Projective warping describes deformation of a flat scene viewed from two angles. It is determined by four GCPs pairs.

The non-vector form of the projective transform is given below.

$$X = \frac{ax + by + c}{gx + hy + 1} \quad (9)$$

$$Y = \frac{dx + ey + f}{gx + hy + 1} \quad (10)$$

This implies the following:

$$X = xa + yb + c - xXg - yXh \quad (11)$$

$$Y = xd + ye + f - xYg - yYh \quad (12)$$

For four points $k = 1, 2, 3, 4$ this can be written:

$$\begin{bmatrix} x_1 & y_1 & 1 & 0 & 0 & 0 & -X_1x_1 & -X_1y_1 \\ x_2 & y_2 & 1 & 0 & 0 & 0 & -X_2x_2 & -X_2y_2 \\ x_3 & y_3 & 1 & 0 & 0 & 0 & -X_3x_3 & -X_3y_3 \\ x_4 & y_4 & 1 & 0 & 0 & 0 & -X_4x_4 & -X_4y_4 \\ 0 & 0 & 0 & x_1 & y_1 & 1 & -Y_1x_1 & -Y_1y_1 \\ 0 & 0 & 0 & x_2 & y_2 & 1 & -Y_2x_2 & -Y_2y_2 \\ 0 & 0 & 0 & x_3 & y_3 & 1 & -Y_3x_3 & -Y_3y_3 \\ 0 & 0 & 0 & x_4 & y_4 & 1 & -Y_4x_4 & -Y_4y_4 \end{bmatrix} \begin{bmatrix} a \\ b \\ c \\ d \\ e \\ f \\ g \\ h \end{bmatrix} = \begin{bmatrix} X_1 \\ X_2 \\ X_3 \\ X_4 \\ Y_1 \\ Y_2 \\ Y_3 \\ Y_4 \end{bmatrix} \quad (13)$$

Which gives in vector form:

$$Av = p \quad (14)$$

When the system is determined (number of points is four), it can be resolved by Gaussian elimination. Our implementation uses singular value decomposition, which can be applied to determined and over determined (more than four points) systems. In the case where more than four GCPs' pairs are available, the result will be a minimisation of the root mean square error.

Some care must be taken when using the singular value decomposition with finite-precision arithmetic. The condition number measures solution sensitivity to finite-precision arithmetic. It is defined as the ratio of the largest singular value to the smallest singular value. If the inverse of this number approach the computer floating point precision, the matrix is said to be ill-conditioned. This is overcome by zeroing singular values that are below a given threshold. The complete derivation of this solution can be found in [23], which is the one implemented in the Interactive Data Language (IDL) used in our implementation.

Projective mapping perfectly warps images of a flat surface viewed by a perfect pinhole camera. It can therefore be used with acceptable error if the situation at hand can be approximated by a flat surface and a perfect camera.

5.2.5.1.2 Polynomial mapping

The polynomial model relates the coordinates of the input image to those of the reference image using a polynomial transformation.

$$X = \sum_{i=0}^N \sum_{j=0}^{N-i} a_{ij} x^i y^j \quad (15)$$

$$Y = \sum_{i=0}^N \sum_{j=0}^{N-i} b_{ij} x^i y^j \quad (16)$$

Coefficients a_{ij} and b_{ij} are usually estimated using GCPs pairs. The method for finding the polynomial coefficients using the GCPs is detailed in [24].

For remote sensing images with small terrain relief and field-of-view, polynomial warping with order N equals to 2 may be sufficient. Polynomial warping of first order cannot cope with terrain relief and changing viewing angle, while polynomial warping of second order second order can map more complex deformations.

The polynomial model exclusively relies on GCPs, order and minimum least-square error to estimate the coordinate transformation. This can result in strange interpolation between GCPs, as there is no constraint other than the order of the polynomial on that interpolation.

5.2.5.2 Local mapping

5.2.5.2.1 Polynomial mapping with image partitioning

Polynomial mapping can easily be modified to perform local mapping by dividing the image into partitions, and applying a polynomial warping to each partition. Figure 16 illustrates the case where an image is divided into four partitions.

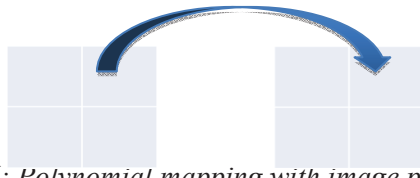


Figure 16: Polynomial mapping with image partitioning

Polynomial mapping with image partitioning is easily applied when point matching is known, as in our simulation. The absence of point matching information would complicate the situation, and an initial coarse mapping could be necessary.

5.2.5.2.2 Piecewise linear mapping

Piecewise linear mapping was first used for image registration by Goshtasby [25]. It consists in two steps:

1. Triangulation of GCPs
2. Local affine transformation for each TP

Triangulation separates reference and target images into corresponding triangular regions. Each TP is mapped from the reference image to the target image by applying the affine transformation that maps the corresponding triangles containing the TP, as shown in figure 17.

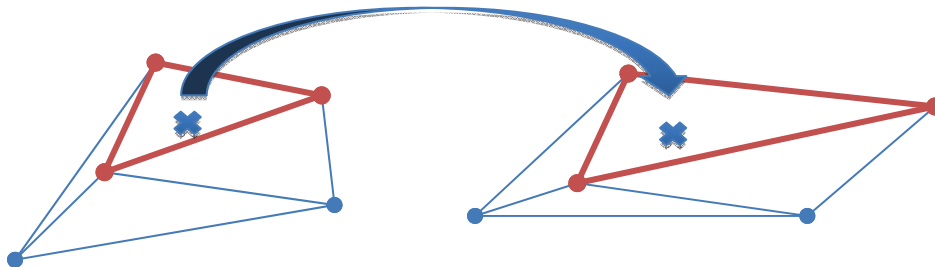


Figure 17: Piecewise linear mapping

Since a local transformation is found for each triangular region, we can expect piecewise linear mapping error to decrease as the number of GCPs increases.

Finding the corresponding triangles for each TP is a compute intense operation that would benefit from parallel execution.

5.2.6 Calculate mapping error on TPs

Mapping error is evaluated using the standard root mean square error (RMSE) on the TPs. The formulas for RMSE computation are given below.

$$RMSE_x = \sqrt{\frac{1}{n} \sum_{i=1}^n (X_i - X_i^R)^2} \quad (17)$$

$$RMSE_y = \sqrt{\frac{1}{n} \sum_{i=1}^n (Y_i - Y_i^R)^2} \quad (18)$$

$$RMSE_{total} = \sqrt{\frac{1}{n} \sum_{i=1}^n [(X_i - X_i^R)^2 + (Y_i - Y_i^R)^2]} \quad (19)$$

Where n is the number of TPs, X_i^R and Y_i^R are coordinates in the reference image, X_i and Y_i are coordinates in the reference image calculated from the sensed image using the transformation model.

5.3 Function for getting mapping error

The methodology presented in the previous section was implemented as an IDL function that gives the mapping error for specific parameters. Actually this function returns mapping error for all implemented mapping algorithms.

```

;+
; :Description:
;   Estimates mapping error for a digital elevation model,
;   looked at from two viewpoints. This function returns the mapping
;   error for a set of mapping algorithms (polynomial, projective,
;   piecewise linear, polynomial with image partitioning).
;
; :Params:
;   DEM : in, required
;       Input DEM, elevation values in metres
;   resdem : in, required
;       DEM resolution, in metres
;   alt : in, required
;       Satellite altitude, in metres
;   ze1 : in, required
;       Zenith of viewpoint 1, in degrees
;   az1 : in, required
;       Azimuth of viewpoint 1, in degrees
;   ze2 : in, required
;       Zenith of viewpoint 2, in degrees
;   az2 : in, required
;       Azimuth of viewpoint 2, in degrees
;   focallength : in, required
;       Focal length of sensor, in metres
;   Numpoints : in, required
;       Number of ground control points by dimension

```

```

;
; :Keywords:
;   CPSELECT : in, optional
;   0 (default) = grid selection of ground control points, 1 = random
;   selection
;   NUMBLOCKS : in, optional
;   Number of blocks for block partitioning algorithms (default = 10)
;   CONSIDEROCCLUSION : in, optional
;   0 (default) = do not consider occlusion, 1 = remove occluded
;   points
;   BLOCKPOLY : in, optional
;   0 (default) = do not calculate mapping error for block polynomial
;   algorithms, 1=do calculate
;   PIECEWISE : in, optional
;   0 (default) = do not calculate mapping error for piecewise linear
;   mapping, 1=do calculate
;   NTESTPOINTS : in, optional
;   Number of test points to use (default = 1000)
;   DEMFILENAME : in, optional
;   Filename of input DEM (used to get occlusion mask, if necessary)
;
; :Author: vlabbe
;-
FUNCTION calculatemappingerror, DEM, resdem, alt, ze1, az1, ze2, az2,
                                focallength, Numpoints,
                                CPSELECT=cpselect,
                                NUMBLOCKS=numblocks,
                                CONSIDEROCCLUSION=ConsiderOcclusion,
                                BLOCKPOLY=blockpoly,
                                PIECEWISE=piecewise,
                                NTESTPOINTS=ntestpoints,
                                DEMFILENAME=DEMFilename

```

This function allows predicting mapping error for a change detection problem involving a pair of images with known acquisition parameters.

5.4 Results

The following mapping error simulation results intend to evaluate the impact of relief on mapping error, and the effect of various parameters like the number of GCPs. The following results present the mapping error as RMSE in normalised image coordinates.

Figure 18 shows the effect of changing the number of partitions on mapping error, for the polynomial mapping with image partitioning algorithm. These results were generated with DEM 3 (Gaspésie, near Murdochville, mountainous relief), zenith angles of 0 and 20 degrees and 160 000 GCPs (400 × 400). The GCPs were generated using a grid and randomly. Mapping error for polynomial mapping algorithms without partitioning are presented as a reference value. Obviously, these algorithms show a constant mapping error versus the number of partitions, and the same mapping error as partitioning algorithms with only one partition. This graphic shows that image partitioning can greatly improve mapping accuracy. Mapping error can be divided by two (degree 2) or by three (degree 1) by dividing the points into many partitions.

Error for polynomial of second order algorithm increases for 100 partitions. This is due to only three tiles, where the algorithm cannot find an adequate second order mapping. Mapping errors on the GCPs for those three tiles are 0.00244786, 0.00103363, 0.00279681. Errors on the TPs are almost the same, which drives the overall error upwards. Note that in the upper graph of Figure 18, the Grid and the Random values are overlapped in most cases, therefore difficult to see, except for the partition poly deg 2 Grid and the partition poly deg 2 Random.

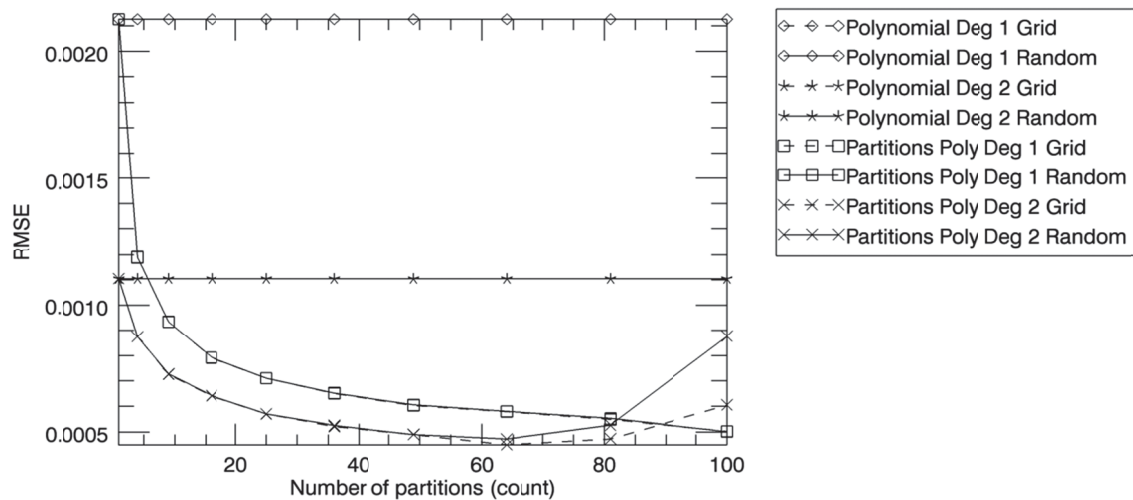


Figure 18: Mapping error vs. number of partitions

Figure 19 presents the mapping error versus the number of GCPs, for a small number of points, for each digital elevation model and for each applicable mapping algorithm. Note that polynomial mapping with image partitioning with 100 partitions cannot be used with 400 GCPs or less. The objective of these graphics is to compare all the algorithms together, and to identify trends. Some results may be difficult to see with precision; Annex B lists all the results in tables.

From figure 19, it can be concluded that random selection of GCPs give the same results as grid selection of GCPs for all algorithms except piecewise linear. This algorithm, when provided with randomly selected GCPs, shows irregular performance as the number of GCPs varies. Since piecewise linear mapping relies on the GCPs (without error minimisation), its performance is highly dependent on them.

For small reliefs, projective and polynomial of second order are better than polynomial of first order. However, as the relief increases, the gap between polynomial of first order and the group of projective and polynomial of second order diminishes. From these results, it can be concluded that when a small number of GCPs is available, it is best to use projective mapping or polynomial of second order mapping.

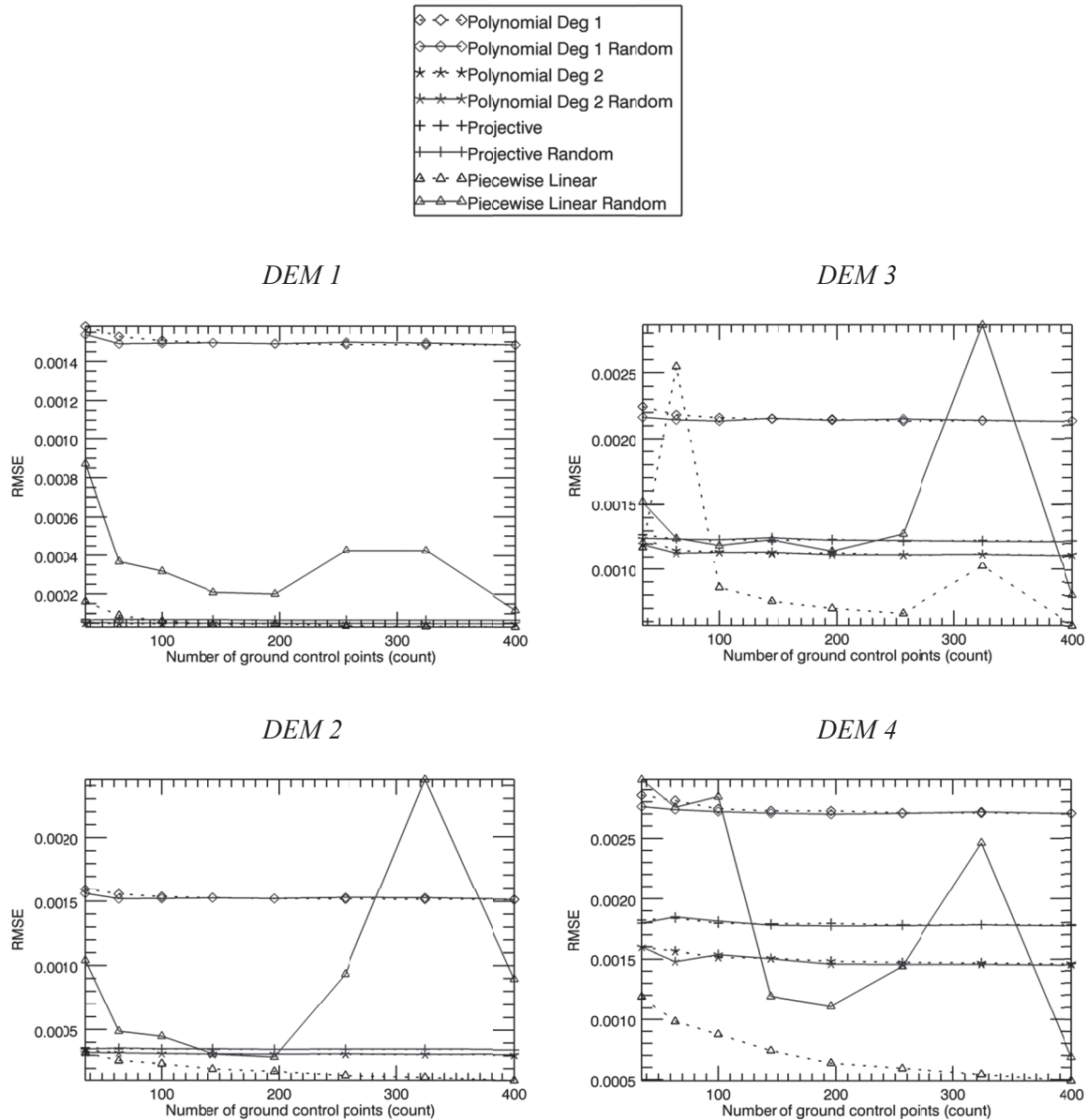


Figure 19: Mapping error vs. number of GCPs (few points)

In figure 20, we can see that, for large numbers of GCPs, the selection method of GCPs has little impact on the mapping error. Piecewise linear mapping performs better with grid-selected GCPs (almost two times better) and displays regular performance. On the other hand, polynomial of second order with partitioning shows irregular performance; a lot of GCPs can lead this algorithm to strange interpolation. We can conclude that piecewise linear mapping is the optimal choice if a large number of GCPs are available.

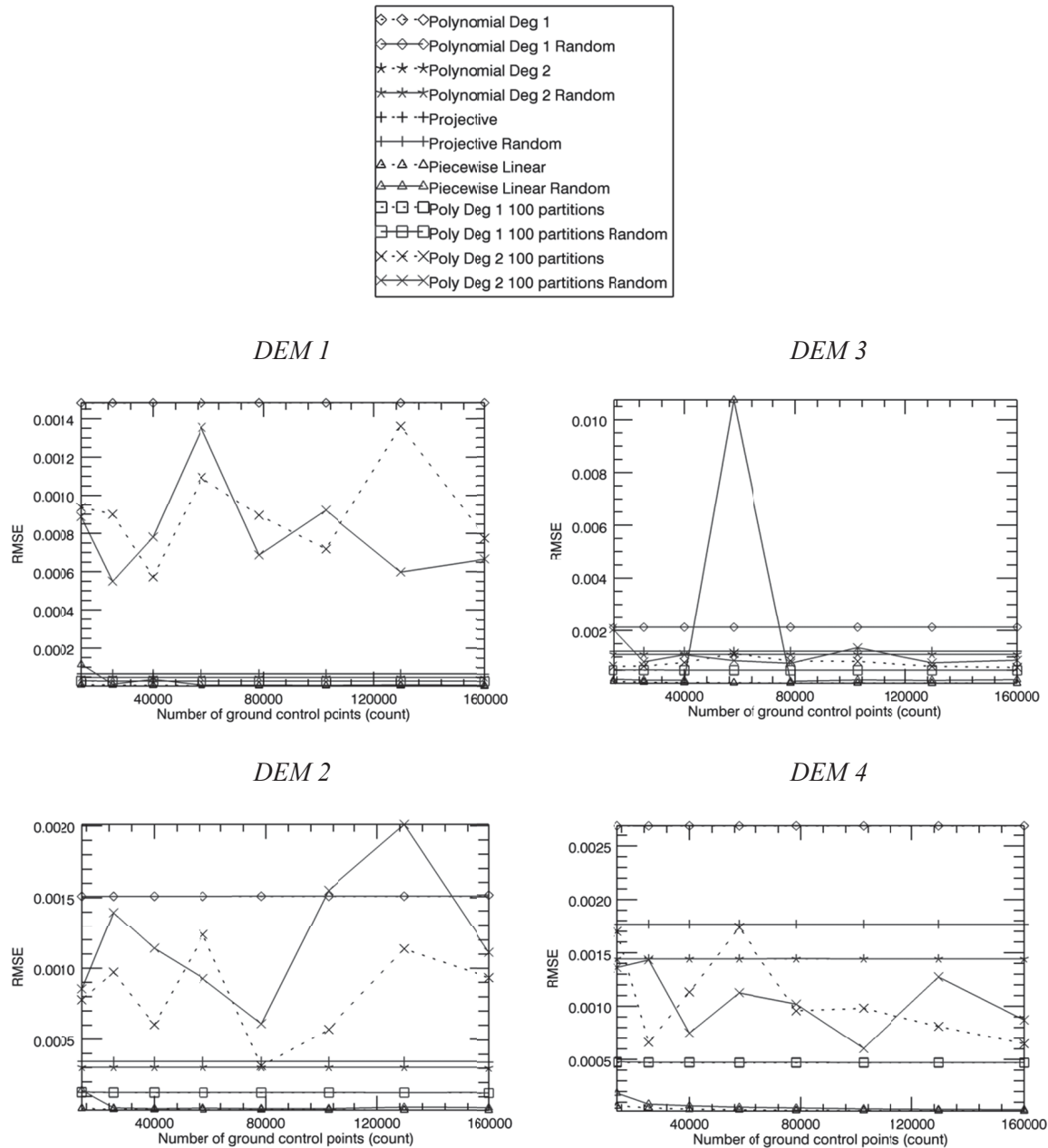


Figure 20: Mapping error vs. number of control points (many points)

In figure 20, DEM 3, piecewise linear mapping visibly underperforms for 57600 GCPs (see Annex B for the detailed results). It was found that only one point was generating this drift. This point is situated outside the convex hull formed by the triangulated control points, and thus the nearest triangle is used to calculate the affine transformation for that point. It so happens that this triangle is formed by almost collinear points, thus generating a large error on the extrapolation for the mapping. This problem can easily be detected by testing all triangles for collinearity. However, it is not easily corrected. It was found that removing one of the collinear points and

triangulating over again makes new collinear points to appear. This can result from the large number of GCPs, or precision of floating point arithmetic operations. This would require further investigation.

Figure 21 and figure 22 combine the results presented before into two graphics (one for grid-selected GCPs and the other for randomly selected GCPs). They show, for each DEM and each number of GCPs, the best mapping algorithm (i.e. the one yielding the smallest mapping error).

In

figure 21, we see that piecewise linear mapping is almost always the best mapping algorithm when the GCPs are selected through a grid. Also, mapping error is greater when there is more relief but this effect can be mitigated by increasing the number of GCPs.

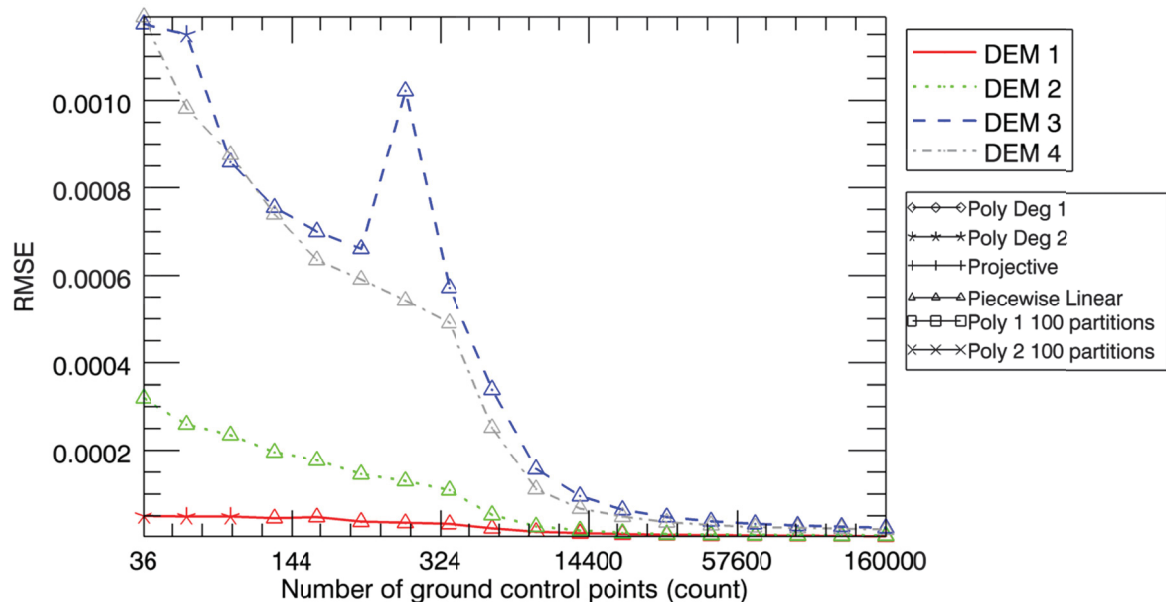


Figure 21: Best mapping error vs. number of GCPs (grid selection)

In figure 22, we can see a cut at around 400 GCPs. For less than 400 GCPs, a polynomial of second order mapping algorithm is in most cases the best choice. However, for more than 400 GCPs, local mapping algorithms are best suited, especially piecewise linear mapping. As relief increases from DEM 1 to DEM 4, so do the mapping error, but again, this is alleviated when the number of GCPs gets higher. The spike at 57600 GCPs was explained in the discussion on figure 20.

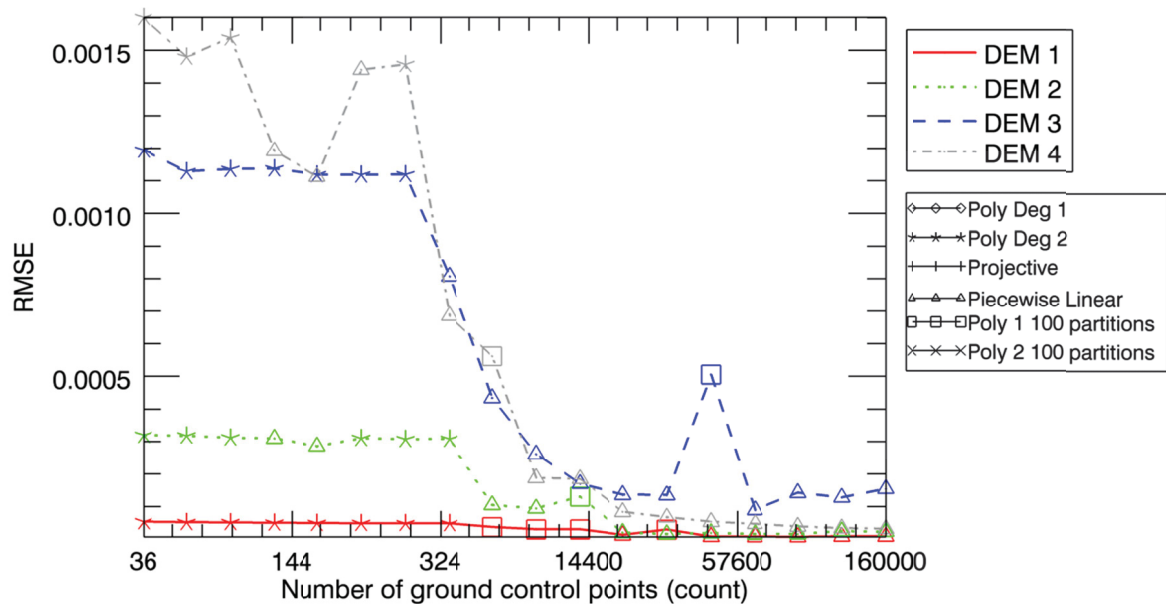


Figure 22: Best mapping error vs. number of GCPs (random selection)

Results from figure 22 are the most significant for the current project, since the only way to get a large number of GCPs is by using automatic detection, which is image content-dependant, resulting in a spatial distribution similar to a random selection. In this figure, we can see that mapping error induced by relief is divided by almost 10 by using local mapping methods supplied with a large number of GPCs. Moreover, for very large number of GCPs, mapping error for terrains with relief can be reduced to levels similar to flat terrains. Table 4 compares smallest mapping error with few GCPs (36) to smallest mapping error with a lot of GCPs (14400). The fourth column shows the increase in error as there is more relief. The fifth column shows that this increase is significantly reduced by using a large number of GCPs. The last column lists the reduction in error caused by increasing the number of GCPs.

Table 4: Mapping error – relief vs. no relief

DEM	Error 36 GCP	Error 14400 GCP	Error 36 GCP / Error 36 GCP DEM1	Error 14400 GCP / Error 36 GCP DEM1	Error reduction (%)
1	5.38E-05	2.99E-05	1	0.6	44
2	0.000320	0.000130	5.9	2.4	59
3	0.001195	0.000170	22.2	3.2	86
4	0.001600	0.000185	29.7	3.4	88

6 Conclusion

A practical method for evaluating registration mapping error was presented. This method relies on a simulation with a digital elevation model to estimate the mapping error of a pair of images, knowing the viewpoints from which the images were acquired. Mapping error evaluation follows these steps: Ground Control Points (GCPs) and Test Points (TPs) selection, occlusion detection, projection to camera plane, mapping parameters estimation using the GCPs and mapping error calculus using the TPs.

The mapping error evaluation method was applied to a test set of digital elevation models showing diverse terrain reliefs: flat, pretty flat, mountainous, and mountainous near a coast. Mapping error was evaluated for four classical mapping algorithms: projective, polynomial, polynomial with image partitioning and piecewise linear. This experiment aimed at finding the best algorithm for each situation. The number and the selection method of GCPs (using a grid or randomly) were also varied.

Random selection of GCPs gives similar results as grid selection for all algorithms except piecewise linear, which is highly dependent on the GCPs selection method. For less than 400 GCPs, polynomial of second order mapping algorithm is in most cases the best choice, with projective mapping close by. For more than 400 GCPs, local mapping algorithms are best suited, especially piecewise linear mapping. As relief increases, so do mapping error, but this is alleviated as the number of GCPs gets higher. Local mapping methods (polynomial with image partitioning and piecewise linear) have shown to reduce the mapping error by more than 80% for mountainous relief. Moreover, for very large number of GCPs, mapping error for terrains with relief can be reduced to levels similar to flat terrains.

This method depends on the availability, resolution and accuracy of the input digital elevation models. Actually, the results presented in this report should be considered optimistic since small relief variations would certainly increase occlusion and add deformation, therefore increasing mapping error. Another consequence of using digital elevation models is that this method cannot be used in an urban context if the digital elevation model does not account for buildings.

This project aims at optimising the use of remote sensing data in the context of change detection. The algorithm presented in this report allows filtering pair of images by estimating their mapping error. It can also be used to plan new missions by predicting mapping error for given conditions.

The first part of this project aimed at predicting image acquisition conditions enabling efficient change detection. Different image acquisition conditions induce geometric errors (overcome by registration) and radiometric errors (overcome by radiometric calibration). The algorithm presented in this report can predict registration mapping error. Radiometric errors, mainly due to difference in scene illumination, also need to be predicted in order to have a complete solution.

The second part of this project will integrate the mapping estimation algorithm into a suite of tools to select pair of images adequate for change detection and acquisition missions planning. By selecting pair of images with low mapping error, the number of false alarms will be reduced. The selected pair of images will be fed to change detection algorithms. Reducing false alarm rates by selecting suitable pair of images can enable automatic processing of a lot of data.

References

- [1] L. Coulter and D. Stow, "Assessment of the Spatial Co-registration of Multitemporal Imagery from Large Format Digital Cameras in the Context of Detailed Change Detection," *Sensors*, vol. 8, pp. 2161-2173, 2008.
- [2] G. Hong and Y. Zhang, "The image registration technique for high resolution remote sensing image in hilly area," 2005.
- [3] M. F. a. A. Yakhdani, A., "Comparative Evaluation Of The Influence Of The Terrain Topography On The Registration Accuracy Of The Fused Multi-sensor Satellite Images (case Study: p5 And P6 Irs Satellite Images)," vol. VCGVA09, 2009.
- [4] L. Brown, "A survey of image registration techniques," *ACM computing surveys (CSUR)*, vol. 24, pp. 325-376, 1992.
- [5] B. Zitova and J. Flusser, "Image registration methods: a survey," *Image and vision computing*, vol. 21, pp. 977-1000, 2003.
- [6] M. Wyawahare, et al., "Image Registration Techniques: An overview," *International Journal of Signal Processing, Image Processing and Pattern Recognition*, vol. 2, pp. 1-5, 2009.
- [7] C. C. o. Geomatics. (2010). *GeoBase Website*. Available: <http://www.geobase.ca/>
- [8] G. o. Canada, et al., "Canadian Digital Elevation Data, Level 1 - Product Specifications," 2007-06-01 2007.
- [9] P. Shirley and S. Marschner, *Fundamentals of computer graphics*: AK Peters, Ltd., 2009.
- [10] W. Strasser, *Schnelle Kurven-und Flächendarstellung auf grafischen Sichtgeräten*: Technische Universität Berlin, 1974.
- [11] M. Ettarid, et al., "Digital true orthophotos generation," 2005.
- [12] J. Rau, et al., "Hidden compensation and shadow enhancement for true orthophoto generation," 2000.
- [13] J. Rau, et al., "True orthophoto generation of built-up areas using multi-view images," *Photogrammetric Engineering and Remote Sensing*, vol. 68, pp. 581-588, 2002.
- [14] Y. Sheng, et al., "True orthoimage production for forested areas from large-scale aerial photographs," *Photogrammetric Engineering and Remote Sensing*, vol. 69, pp. 259-266, 2003.
- [15] A. Habib, et al., "New methodologies for true orthophoto generation," *Photogrammetric Engineering and Remote Sensing*, vol. 73, p. 25, 2007.
- [16] S. Roth, "Ray casting for modeling solids," *Computer Graphics and Image Processing*, vol. 18, pp. 109-144, 1982.
- [17] ITTIVS, "IDL ", 7.1.1 ed: ITTIVS, 2009.
- [18] P. Messmer, et al., "GPULib: GPU computing in high-level languages," *Computing in Science and Engineering*, vol. 10, pp. 70-73, 2008.
- [19] NVIDIA, "Compute Unified Device Architecture Programming Guide Version 3.2," NVIDIA: Santa Clara, CA, 2010.
- [20] M. Obeysekera, "Affine Reconstruction from multiple views using Singular Value Decomposition," 2008.
- [21] I. T. Young, et al., *Fundamentals of image processing*: Citeseer, 1995.
- [22] B. Jähne, "Digital Image Processing. 2002," ed: Springer-Verlag Berlin, Inc., ISBN.
- [23] W. H. Press, et al., "Numerical recipes in C," 1992.

- [24] R. Schowengerdt, *Remote sensing: models and methods for image processing*: Academic Pr, 2007.
- [25] A. Goshtasby, "*Piecewise linear mapping functions for image registration*," Pattern Recognition, vol. 19, pp. 459-466, 1986.

Annex A Effet of Earth curvature on simulation

A.1 Satellite position

Since the satellite is expected to have a constant altitude, it is necessary to consider Earth curvature when the satellite is looking at the scene from an off-nadir view angle, as illustrated in Figure A-1. Angle α is the off-nadir view angle of the satellite, H its altitude and R the radius of the Earth.

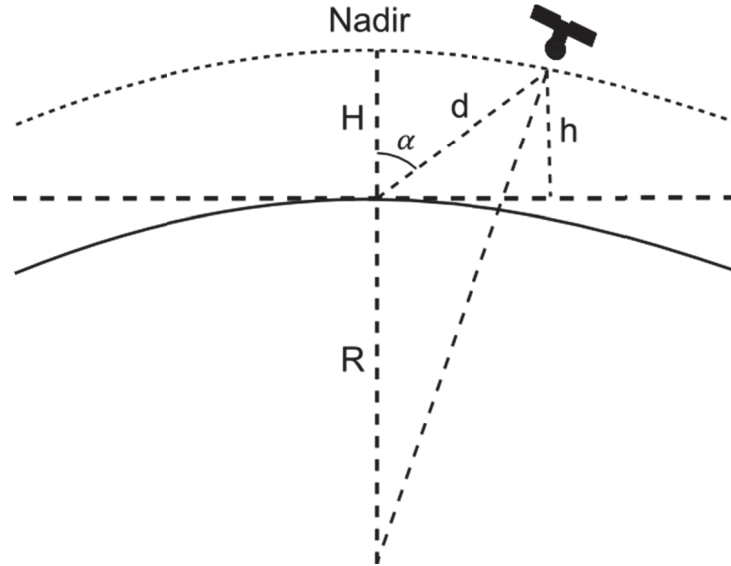


Figure A-1: Satellite position considering Earth curvature

It is easy to calculate the satellite 3D position using the law of cosines with the triangle formed by sides R , d , and $R + H$, and angle $180 - \alpha$, as shown in Figure A-2.

$$d = R \cos(180 - \alpha) \pm \sqrt{(R + H)^2 - R^2 \sin^2(180 - \alpha)} \quad (\text{A.1})$$

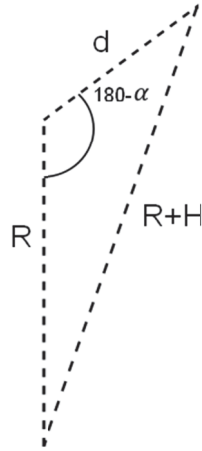


Figure A-2: Satellite distance using law of cosines

Knowing d , h can be calculated using

$$h = \sin(90 - \alpha) * d \quad (\text{A.2})$$

A.2 Digital elevation model

To evaluate the effect of Earth curvature on occlusion detection and projected 2D coordinates, we proceed in two steps: first we calculate 3D coordinates with and without Earth curvature consideration; second we calculate the difference for 2D projected coordinates. We approximate Earth as locally spherical, even if digital ground elevations are provided for an ellipsoidal Earth surface model.

Figure A-3 defines the geometrical variables necessary to the calculation of 3D coordinates considering Earth curvature (x, z) and neglecting it (x', z') . We simplify the problem by working in 2D but the results are easily extendable to 3D.

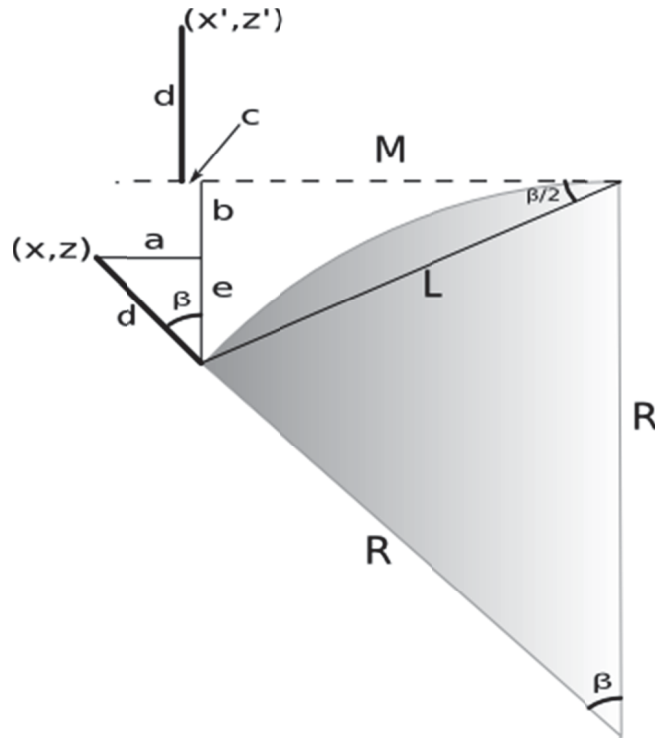


Figure A-3: Earth curvature effect on ground elevation values

Displacement in z is given by:

$$z' - z = b + e \quad (\text{A.3})$$

And b by

$$b + e = L * \sin\left(\frac{\beta}{2}\right) \quad (\text{A.4})$$

Where

$$L = \frac{R * \sin(\beta)}{\sin(90 - \frac{\beta}{2})} \quad (\text{A.5})$$

Displacement in x is given by:

$$x - x' = a - c \quad (\text{A.6})$$

where a is calculated by

$$a = d * \sin(\beta) \quad (\text{A.7})$$

and c by

$$c = M - L * \cos\left(\frac{\beta}{2}\right) \quad (\text{A.8})$$

For the datasets used in this experiment, we have the following values:

1. $R = 6\,378\,137$ meters
2. DEM data are 1201×1201 pixels, spaced by 0.75 arc-second.

Suppose a pixel at DEM border, i.e. position [1200, 1200, 1000m]. According to formulae presented before, this yields X,Y,Z displacements of 0.00021691279, 0.00021691279, and 1.3089958 pixel. For the purpose of occlusion detection described here, X and Y displacements are negligible, and Z displacement can also be neglected since occlusion detection is only used as an indicator for performance prediction.

Annex B Results

This annex presents in tables the mapping error results shown in graphics in section 5.4.

B.1 Number of partitions

Table B- presents the mapping error for four mapping algorithms as a function of the number of blocks (or partitions).

Table B-1: Estimated mapping error vs. Number of partitions

Blocks	Poly 1 grid	Poly 2 grid	Partitions Poly 1 grid	Partitions Poly 2 grid	Poly 1 random	Poly 2 random	Partitions Poly 1 random	Partitions Poly 2 random
1	0.002126	0.001105	0.002126	0.001105	0.002127	0.001105	0.002127	0.001105
4	0.002126	0.001105	0.001189	0.000875	0.002127	0.001105	0.001190	0.000875
9	0.002126	0.001105	0.000934	0.000726	0.002127	0.001105	0.000934	0.000727
16	0.002126	0.001105	0.000792	0.000641	0.002127	0.001105	0.000792	0.000642
25	0.002126	0.001105	0.000711	0.000570	0.002127	0.001105	0.000711	0.000569
36	0.002126	0.001105	0.000651	0.000520	0.002127	0.001105	0.000652	0.000525
49	0.002126	0.001105	0.000603	0.000490	0.002127	0.001105	0.000605	0.000489
64	0.002126	0.001105	0.000579	0.000449	0.002127	0.001105	0.000580	0.000472
81	0.002126	0.001105	0.000548	0.000472	0.002127	0.001105	0.000552	0.000526
100	0.002126	0.001105	0.000502	0.000605	0.002127	0.001105	0.000501	0.000877

B.2 Number of points

Table B-2 to table b-9 present the mapping errors for all applicable mapping algorithms as a function of the number of ground control points (GCPS), for all four digital elevation models of the test set.

B.2.1 Small number of GCPs

Table B-2: Estimated mapping error for DEM 1 – small number of GCPs

Control Points	Poly 1 Grid	Poly 2 Grid	Projective Grid	Piecewise linear grid	Poly 1 Random	Poly 2 Random	Projective Random	Piecewise linear Random
36	0.001581	4.99E-05	6.93E-05	0.000161	0.001539	5.38E-05	6.77E-05	0.000873
64	0.001528	4.84E-05	6.76E-05	8.96E-05	0.001491	5.16E-05	6.98E-05	0.000367
100	0.001507	4.84E-05	6.71E-05	6.17E-05	0.001494	5.12E-05	6.86E-05	0.000317
144	0.001496	4.79E-05	6.70E-05	4.47E-05	0.001496	5.00E-05	6.80E-05	0.000208
196	0.001491	4.89E-05	6.61E-05	4.72E-05	0.001490	4.88E-05	6.66E-05	0.000200
256	0.001487	4.79E-05	6.62E-05	3.65E-05	0.001498	4.86E-05	6.62E-05	0.000426
324	0.001486	4.79E-05	6.61E-05	3.39E-05	0.001495	4.84E-05	6.62E-05	0.000425
400	0.001484	4.78E-05	6.60E-05	3.14E-05	0.001485	4.79E-05	6.60E-05	0.000117

Table B-3: Estimated mapping error for DEM 2 – small number of GCPs

Control Points	Poly 1 Grid	Poly 2 Grid	Projective Grid	Piecewise linear grid	Poly 1 Random	Poly 2 Random	Projective Random	Piecewise linear Random
36	0.001598	0.000342	0.000358	0.000319	0.001561	0.00032	0.000348	0.001041
64	0.001556	0.000319	0.000350	0.000259	0.001519	0.000318	0.000355	0.000486
100	0.001535	0.000312	0.000348	0.000235	0.001521	0.000312	0.000349	0.000448
144	0.001527	0.000308	0.000346	0.000195	0.001525	0.000311	0.000350	0.000310
196	0.001520	0.000308	0.000346	0.000177	0.001521	0.000309	0.000347	0.000286
256	0.001517	0.000307	0.000346	0.000145	0.001529	0.000310	0.000347	0.000933
324	0.001515	0.000306	0.000346	0.000129	0.001526	0.000307	0.000347	0.002447
400	0.001513	0.000304	0.000345	0.000109	0.001516	0.000308	0.000346	0.000894

Table B-4: Estimated mapping error for DEM 3 – small number of GCPs

Control Points	Poly 1 Grid	Poly 2 Grid	Projective Grid	Piecewise linear grid	Poly 1 Random	Poly 2 Random	Projective Random	Piecewise linear Random
36	0.002245	0.001238	0.001270	0.001173	0.002165	0.001195	0.001243	0.001517
64	0.002183	0.001149	0.001236	0.002548	0.002145	0.001128	0.001236	0.001243
100	0.002160	0.001139	0.001232	0.000858	0.002137	0.001135	0.001232	0.001187
144	0.002152	0.001125	0.001226	0.000754	0.002157	0.001137	0.001248	0.001232
196	0.002150	0.001133	0.001233	0.000700	0.002143	0.001118	0.001228	0.001144
256	0.002135	0.001113	0.001220	0.000661	0.002151	0.001118	0.001227	0.001277
324	0.002139	0.001121	0.001226	0.001022	0.002142	0.001119	0.001219	0.002863
400	0.002132	0.001112	0.001220	0.000572	0.002131	0.001110	0.001217	0.000807

Table B-5: Estimated mapping error for DEM 4 – small number of GCPs

Control Points	Poly 1 Grid	Poly 2 Grid	Projective Grid	Piecewise linear grid	Poly 1 Random	Poly 2 Random	Projective Random	Piecewise linear Random
36	0.002854	0.001599	0.001821	0.001189	0.002761	0.001600	0.001795	0.002984
64	0.002810	0.001564	0.001836	0.000982	0.002735	0.001480	0.001847	0.002754
100	0.002741	0.001516	0.001795	0.000875	0.002719	0.001538	0.001812	0.002842
144	0.002725	0.001508	0.001788	0.000739	0.002706	0.001505	0.001779	0.001192
196	0.002724	0.001484	0.001794	0.000635	0.002697	0.001459	0.001771	0.001112
256	0.002708	0.001473	0.001781	0.000591	0.002704	0.001457	0.001775	0.001440
324	0.002707	0.001469	0.001782	0.000542	0.002717	0.001457	0.001782	0.002464
400	0.002703	0.001461	0.001782	0.000490	0.002701	0.001450	0.001773	0.000686

B.2.2 Large number of GCPs

Table B-6: Estimated mapping error for DEM 1 – large number of GCPs

Control Points	Poly 1 Grid	Poly 2 Grid	Proj Grid	PI grid	Poly 1 blocks grid	Poly 2 blocks grid	Poly 1 Rand	Poly 2 Rand	Proj Rand	PI Rand	Poly 1 blocks Rand	Poly 2 blocks Rand
14400	0.001482	4.77E-05	6.58E-05	1.03E-05	2.91E-05	0.000937	0.001483	4.77E-05	6.58E-05	0.000114	2.99E-05	0.000887
25600	0.001482	4.78E-05	6.58E-05	8.27E-06	2.90E-05	0.000900	0.001483	4.77E-05	6.58E-05	1.28E-05	2.94E-05	0.000550
40000	0.001482	4.78E-05	6.58E-05	6.76E-06	2.90E-05	0.000573	0.001483	4.77E-05	6.58E-05	3.73E-05	2.92E-05	0.000781
57600	0.001482	4.78E-05	6.58E-05	5.82E-06	2.89E-05	0.001093	0.001483	4.77E-05	6.58E-05	8.02E-06	2.91E-05	0.001354
78400	0.001482	4.78E-05	6.58E-05	5.36E-06	2.89E-05	0.000895	0.001483	4.78E-05	6.58E-05	7.62E-06	2.91E-05	0.000687
102400	0.001482	4.78E-05	6.58E-05	4.77E-06	2.89E-05	0.000718	0.001483	4.78E-05	6.58E-05	7.10E-06	2.91E-05	0.000922
129600	0.001482	4.78E-05	6.58E-05	4.20E-06	2.89E-05	0.001361	0.001483	4.78E-05	6.58E-05	8.87E-06	2.90E-05	0.000598
160000	0.001482	4.78E-05	6.58E-05	3.58E-06	2.89E-05	0.000775	0.001483	4.78E-05	6.58E-05	8.77E-06	2.89E-05	0.000666

Table B-7: Estimated mapping error for DEM 2 – large number of GCPs

Control Points	Poly 1 Grid	Poly 2 Grid	Proj Grid	PI grid	Poly 1 blocks grid	Poly 2 blocks grid	Poly 1 Rand	Poly 2 Rand	Proj Rand	PI Rand	Poly 1 blocks Rand	Poly 2 blocks Rand
14400	0.001510	0.000303	0.000345	1.69E-05	0.000128	0.000778	0.001511	0.000303	0.000345	0.000142	0.000130	0.000854
25600	0.001510	0.000303	0.000345	1.09E-05	0.000127	0.000972	0.001511	0.000303	0.000345	1.95E-05	0.000127	0.001396
40000	0.001511	0.000303	0.000345	8.35E-06	0.000126	0.000603	0.001511	0.000303	0.000345	1.56E-05	0.000128	0.001140
57600	0.001511	0.000303	0.000345	7.37E-06	0.000126	0.001236	0.001511	0.000303	0.000345	1.88E-05	0.000127	0.000926
78400	0.001511	0.000303	0.000345	6.73E-06	0.000126	0.000313	0.001512	0.000303	0.000345	1.52E-05	0.000126	0.000610
102400	0.001511	0.000303	0.000345	6.01E-06	0.000126	0.000569	0.001512	0.000303	0.000345	1.56E-05	0.000126	0.001551
129600	0.001511	0.000303	0.000345	5.65E-06	0.000126	0.001135	0.001512	0.000303	0.000345	2.44E-05	0.000126	0.002010
160000	0.001511	0.000303	0.000345	5.54E-06	0.000126	0.000933	0.001512	0.000303	0.000345	2.26E-05	0.000126	0.001112

Table B-8: Estimated mapping error for DEM 3 – large number of GCPs

Control Points	Poly 1 Grid	Poly 2 Grid	Proj Grid	PI grid	Poly 1 blocks grid	Poly 2 blocks grid	Poly 1 Rand	Poly 2 Rand	Proj Rand	PI Rand	Poly 1 blocks Rand	Poly 2 blocks Rand
14400	0.002126	0.001105	0.001216	9.51E-05	0.000503	0.000648	0.002126	0.001105	0.001216	0.000170	0.000510	0.002076
25600	0.002126	0.001105	0.001216	6.37E-05	0.000503	0.000652	0.002126	0.001105	0.001216	0.000136	0.000508	0.000816
40000	0.002126	0.001105	0.001216	4.72E-05	0.000502	0.000791	0.002126	0.001105	0.001216	0.000135	0.000507	0.001084
57600	0.002126	0.001105	0.001216	3.76E-05	0.000503	0.001132	0.002126	0.001105	0.001216	0.010744	0.000505	0.000864
78400	0.002126	0.001105	0.001216	3.16E-05	0.000502	0.000854	0.002127	0.001105	0.001216	8.90E-05	0.000503	0.000763
102400	0.002126	0.001105	0.001216	2.75E-05	0.000502	0.000834	0.002127	0.001105	0.001216	0.000142	0.000502	0.001349
129600	0.002126	0.001105	0.001216	2.53E-05	0.000502	0.000644	0.002127	0.001105	0.001216	0.000128	0.000502	0.000779
160000	0.002126	0.001105	0.001216	2.24E-05	0.000502	0.000605	0.002127	0.001105	0.001216	0.000154	0.000501	0.000877

Table B-9: Estimated mapping error for DEM 4 – large number of GCPs

Control Points	Poly 1 Grid	Poly 2 Grid	Proj Grid	PI grid	Poly 1 blocks grid	Poly 2 blocks grid	Poly 1 Rand	Poly 2 Rand	Proj Rand	PI Rand	Poly 1 blocks Rand	Poly 2 blocks Rand
14400	0.002688	0.001443	0.001768	6.65E-05	0.000471	0.001700	0.002688	0.001443	0.001767	0.000185	0.000480	0.001362
25600	0.002688	0.001443	0.001768	4.81E-05	0.000470	0.000659	0.002688	0.001443	0.001767	8.36E-05	0.000475	0.001432
40000	0.002688	0.001443	0.001768	3.52E-05	0.000470	0.001132	0.002688	0.001443	0.001767	6.68E-05	0.000475	0.000748
57600	0.002688	0.001443	0.001768	2.90E-05	0.000469	0.001737	0.002688	0.001443	0.001768	5.33E-05	0.000474	0.001125
78400	0.002688	0.001443	0.001768	2.42E-05	0.000470	0.000957	0.002689	0.001444	0.001768	4.67E-05	0.000474	0.001019
102400	0.002688	0.001443	0.001768	2.25E-05	0.000469	0.000980	0.002689	0.001444	0.001767	3.85E-05	0.000473	0.000603
129600	0.002688	0.001443	0.001768	2.04E-05	0.000469	0.000810	0.002688	0.001443	0.001767	3.35E-05	0.000472	0.001273
160000	0.002688	0.001443	0.001768	1.87E-05	0.000469	0.000647	0.002688	0.001443	0.001767	3.16E-05	0.000472	0.000871

This page intentionally left blank.

List of symbols/abbreviations/acronyms/initialisms

2D	Two-dimension
2.5D	Two-and-a-half dimension, used to talk about digital elevation models, which does not give a complete 3D representation, but discrete elevation values sampled at a given ground distance.
3D	Three-dimension
CCOG	Canadian Council on Geomatics
CDED	Canadian Digital Elevation Data
DEM	Digital elevation model
GCP	Ground control points
IDL	Interactive Data Language
NAD83	North American Datum 1983
RMSE	Root mean square error
TP	Test points

This page intentionally left blank.

DOCUMENT CONTROL DATA		
(Security markings for the title, abstract and indexing annotation must be entered when the document is Classified or Designated)		
1. ORIGINATOR (The name and address of the organization preparing the document. Organizations for whom the document was prepared, e.g. Centre sponsoring a contractor's report, or tasking agency, are entered in section 8.) AEREX Avionics Inc. 324, Saint-Augustin Avenue Breakeyville (Québec) G0S 1E1		2a. SECURITY MARKING (Overall security marking of the document including special supplemental markings if applicable.) UNCLASSIFIED
		2b. CONTROLLED GOODS (NON-CONTROLLED GOODS) DMC A REVIEW: GCEC JUNE 2010
3. TITLE (The complete document title as indicated on the title page. Its classification should be indicated by the appropriate abbreviation (S, C or U) in parentheses after the title.) Prediction of Image Registration Performance : Final Report		
4. AUTHORS (last name, followed by initials – ranks, titles, etc. not to be used) Labbé, V.		
5. DATE OF PUBLICATION (Month and year of publication of document.) March 2012	6a. NO. OF PAGES (Total containing information, including Annexes, Appendices, etc.) 60	6b. NO. OF REFS (Total cited in document.) 25
7. DESCRIPTIVE NOTES (The category of the document, e.g. technical report, technical note or memorandum. If appropriate, enter the type of report, e.g. interim, progress, summary, annual or final. Give the inclusive dates when a specific reporting period is covered.) Contract Report		
8. SPONSORING ACTIVITY (The name of the department project office or laboratory sponsoring the research and development – include address.) Defence Research and Development Canada – Valcartier 2459 Pie-XI Blvd North Quebec (Quebec) G3J 1X5 Canada		
9a. PROJECT OR GRANT NO. (If appropriate, the applicable research and development project or grant number under which the document was written. Please specify whether project or grant.)	9b. CONTRACT NO. (If appropriate, the applicable number under which the document was written.) W7701-092854/001/QCL	
10a. ORIGINATOR'S DOCUMENT NUMBER (The official document number by which the document is identified by the originating activity. This number must be unique to this document.) 2011-92854-2	10b. OTHER DOCUMENT NO(s). (Any other numbers which may be assigned this document either by the originator or by the sponsor.) DRDC Valcartier CR 2013-036	
11. DOCUMENT AVAILABILITY (Any limitations on further dissemination of the document, other than those imposed by security classification.) Unlimited		
12. DOCUMENT ANNOUNCEMENT (Any limitation to the bibliographic announcement of this document. This will normally correspond to the Document Availability (11). However, where further distribution (beyond the audience specified in (11) is possible, a wider announcement audience may be selected.) Unlimited		

13. **ABSTRACT** (A brief and factual summary of the document. It may also appear elsewhere in the body of the document itself. It is highly desirable that the abstract of classified documents be unclassified. Each paragraph of the abstract shall begin with an indication of the security classification of the information in the paragraph (unless the document itself is unclassified) represented as (S), (C), (R), or (U). It is not necessary to include here abstracts in both official languages unless the text is bilingual.)

This report presents a practical method for estimating registration mapping error for a given relief and satellite attitudes. This method relies on a simulation using a digital elevation model to calculate the mapping error for a set of parameters. The method was applied to a test set of digital elevation models showing diverse terrain reliefs: flat, pretty flat, mountainous, and mountainous near a coast. Mapping error increases for terrains with more relief; but this error can be reduced by using local mapping algorithms, which were found to decrease mapping error for mountainous regions by 80%. Our method quantifies the mapping error and compares the mapping error for diverse conditions. These results can then be used to delimit the change detection capability and to better plan future image acquisition missions.

Ce rapport présente une méthode permettant d'estimer l'erreur de mappage, lors du recalage, pour un relief et des positions de satellite donnés. Cette méthode se base sur une simulation utilisant un modèle altimétrique numérique afin de calculer l'erreur de mappage pour un ensemble de paramètres. Cette méthode fut appliquée à un ensemble de modèles altimétriques numériques de test comportant divers types de reliefs : plat, presque plat, montagneux, montagneux près d'une côte. Évidemment, l'erreur de mappage croît pour les terrains comportant plus de relief, mais cette erreur peut être réduite en utilisant des algorithmes de mappage local. On a estimé que les algorithmes de mappage local font diminuer l'erreur de mappage dans les régions montagneuses de 80%. Notre méthode permet de quantifier l'erreur de mappage et de comparer les erreurs de mappage pour différentes conditions. Ces résultats peuvent alors servir à délimiter les capacités des algorithmes de détection de changement et à mieux planifier de futures missions d'acquisition de données.

14. **KEYWORDS, DESCRIPTORS or IDENTIFIERS** (Technically meaningful terms or short phrases that characterize a document and could be helpful in cataloguing the document. They should be selected so that no security classification is required. Identifiers, such as equipment model designation, trade name, military project code name, geographic location may also be included. If possible keywords should be selected from a published thesaurus, e.g. Thesaurus of Engineering and Scientific Terms (TEST) and that thesaurus identified. If it is not possible to select indexing terms which are Unclassified, the classification of each should be indicated as with the title.)

images coregistration; performance prediction; images warping; registration; geometric correction; digital elevation models; ground control points (GCPs); Geobase; earth curvature; satellite

Defence R&D Canada

Canada's Leader in Defence
and National Security
Science and Technology

R & D pour la défense Canada

Chef de file au Canada en matière
de science et de technologie pour
la défense et la sécurité nationale



www.drdc-rddc.gc.ca